

A Two-Phase Model to Investigate LDL Toxicity in Early Atherosclerosis

Abdush Salam Pramanik^{*1}, Bibaswan Dey^{†1}, and G. P. Raja Sekhar^{‡2}

¹Department of Mathematics, University of North Bengal, Raja Rammohunpur, Darjeeling-734013, West Bengal, India.

²Department of Mathematics, Indian Institute of Technology Kharagpur, Kharagpur-721302, West Bengal, India.

Abstract

Atherosclerosis is a chronic inflammatory cardiovascular disease in which fatty plaque is built inside an artery wall. Early atherosclerotic plaque development is typically characterised by inflammatory tissues primarily consisting of foam cells and macrophages. We present a multiphase model that explores early plaque growth to emphasise the role of cytokines (in particular, Monocyte Chemoattractant Protein-1) and oxidised low-density lipoprotein (oxLDL) in monocyte recruitment and foam cell production, respectively. The plaque boundary is assumed to move at the same speed as the inflammatory tissues close to the periphery. This study discusses oxLDL-induced toxic environment towards macrophages and foam cells such that they start to die beyond a threshold limit of oxLDL concentration owing to excessive consumption. Our findings reveal that initially, the plaque evolves rapidly, and the growth rate subsequently reduces with time because of oxLDL-induced toxicity. In addition, it is observed that the saturation of inflammatory cell volume fraction becomes independent of oxLDL concentration beyond the threshold limit, referred to as the oxLDL toxicity limit. Our study manifests that a higher flux of oxLDL leads to plaque growth decay, whereas an increase in cytokines flux is favourable for enhanced plaque growth. Detailed analysis of the model presented in this article unfolds critical insights into the various biochemical and cellular mechanisms behind early plaque development.

Keywords: oxidised LDL (oxLDL); Functional Cytokines (f-cytokines); Macrophage; Foam Cell; Perturbation Approximation; Mixture Theory.

*Electronic address: rs_abdush@nbu.ac.in

†Electronic address (Corresponding Author): bibaswandey@nbu.ac.in

‡Electronic address: rajas@iitkgp.ac.in

1 Introduction

Cardiovascular diseases (CVDs) have become a major warning to human health and a leading cause of loss of life worldwide [53]. Atherosclerosis, a type of CVD, is an inflammatory disease associated with an excess concentration of low-density lipoprotein (LDL) in the bloodstream. Typical risk factors such as hypertension, smoking, diabetes, hyperlipidemia, etc., can result in a dreadful situation for a person having atherosclerosis [18]. Primarily, atherosclerosis occurs within bifurcated large and medium arteries, particularly at the position of curvature where a low value of endothelium shear stress is anticipated [13]. The plaque formation begins with the deposition of sizeable lipid-laden foam cells derived from monocytes which phagocytose oxidized low-density lipoprotein (oxLDL) present within intima [41]. In due course of time, such a plaque becomes stiff and unstable so that it can rupture. Subsequently, blood clots develop at the ruptured portion of the plaque and can block blood flow, resulting in myocardial infarction, ischemic cerebral stroke, etc. [29]. Plaque formation is almost asymptomatic in a patient with atherosclerosis unless diagnosed clinically [19]. Hence it is essential to detect the plaque at an early stage in order to prevent above mentioned fatal health complications. Therefore, a complete understanding of plaque growth in early atherosclerosis is crucial.

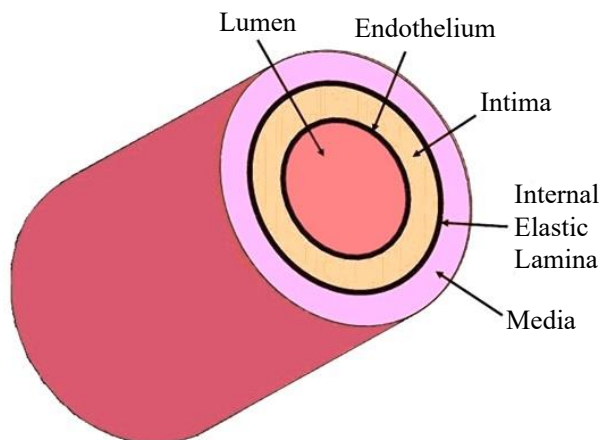


Figure 1: Cross-section of a healthy artery showing the artery wall consists of different cell layers. The innermost layer of the wall is comprised of a thin sheet of endothelium cells, called *the endothelium*. The endothelium forms an interface between the blood flow in the lumen and the rest of the artery wall. Immediately beneath the endothelium, a thin tissue layer lies called the *intima*. The underlying tissue layer is said to be *media* which is separated from the intima by a dense tissue membrane known as *internal elastic lamina (IEL)*.

Early atherosclerotic plaque develops in the narrow intimal layer of an artery. Figure 1 depicts the layered structure of a healthy artery wall. When there is turbulence or recirculation in the blood flow into the lumen region, the endothelium gets damaged, particularly

in areas of low shear stress. Several factors, such as hypertension, smoking, consuming processed foods and alcohol etc., expedite endothelium damage [12, 25]. Low-density lipoprotein (LDL) from the bloodstream penetrates the artery wall to enter the intima through the injured endothelium. Inside intima, LDL molecules are modified by free oxygen radicals to become oxidized LDL (oxLDL) [43, 16]. The presence of oxLDL enables endothelium cells to secrete monocyte chemotactic protein-1 (MCP-1) and monocyte colony-stimulating factor (M-CSF) [57]. In addition, the endothelium in the vicinity of oxLDL expresses leukocyte adhesion molecules on the surface of the endothelium, such as vascular cell adhesion molecule-1 (VCAM-1) and intracellular adhesion molecules (ICAM-1) [41, 29]. These adhesion molecules allow monocytes from the bloodstream to attach to the endothelium surface [43]. The monocytes enter the intima in response to chemoattractant gradients like MCP-1 and other cytokines [28, 29, 43]. Subsequently, monocytes differentiate into macrophages inside the intima in response to M-CSF [52, 41]. Macrophages within the intima consume oxLDL, which causes them to become large, lipid-laden foam cells [43, 8, 27, 31]. Consequently, several foam cells produced with macrophages form an early plaque in atherosclerosis [11]. At this early stage (early atherosclerosis), two essential components of the formed plaque are foam cells and macrophages. These foam cells further secrete more chemoattractants and cytokines to attract more monocytes into the intima [10, 52]. Although the death of macrophages and foam cells is not excessively studied, some studies describe the possible cause of death. According to Marchant et al. [44], macrophages die due to the toxic environment induced by oxLDL. In addition, foam cells die due to the extensive consumption of oxLDL [32, 42]. Consequently, a threshold value of oxLDL concentration exists, after which inflammatory cells (macrophages, foam cells) start to die [42]. The dead foam cells within plaque release oxLDL and other cellular debris [3]. Macrophages consume more oxLDL and produce new foam cells. Figure 2 outlines the plaque formation at an early stage in a schematic diagram.

In the next stage, smooth muscle cells (SMCs) within the media region migrate through the IEL to the intima. The proliferation of SMCs is induced by growth factors like platelet-derived growth factor (PDGF) secreted from the endothelium and foam cells [49]. In addition, SMCs produce collagen, which is upregulated by a cytokine transforming growth factor-beta ($TGF-\beta$) released by foam cells, SMCs and endothelium cells [30]. Migrated SMCs and Collagen form a cap formation near the endothelium regarded as fibrous cap [49]. At this stage, the plaque becomes more arduous and is viewed as advanced atherosclerotic plaque. However, we intend to focus on early-stage plaque formation formed by the foam cells and macrophages. Hence, we aim to develop a mathematical model to describe plaque growth and the corresponding biochemical mechanism where the plaque boundary evolves with time.

Various mathematical models have been developed to understand the early stage of atherosclerosis with a specific focus. For example, Cobbold et al. [16] proposed a mathematical model for LDL oxidation using ordinary differential equations (ODEs) based on in-vitro experimental data. The presence of LDL, more precisely oxidized LDL, arises to be a vital factor of the

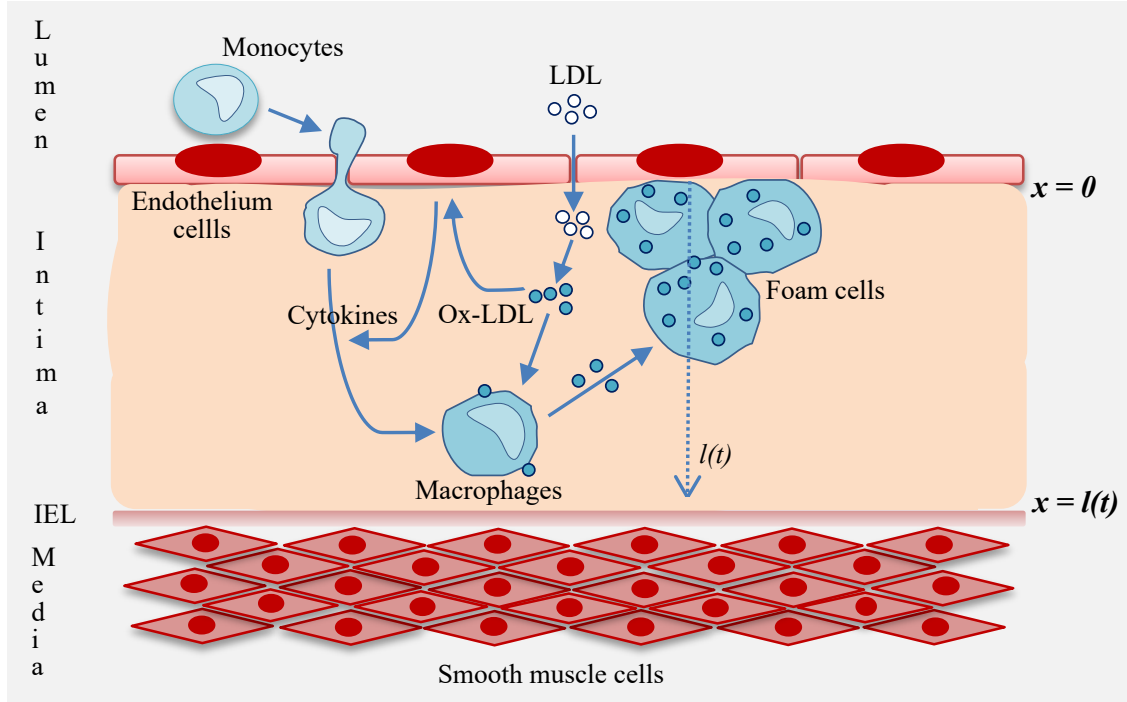


Figure 2: Schematic diagram of the key processes in plaque formation at the early stage. Low-density lipoprotein (LDL), which is present in the bloodstream, enters the intima through the damaged endothelium and undergoes modification to become oxidized LDL (oxLDL). OxLDL induces the secretion of several cytokines from the endothelium cells, including monocyte chemoattractant protein-1 (MCP-1), monocyte colony-stimulating factor (M-CSF), and ES-cytokines. In response to the cytokines, particularly for MCP-1, monocytes adhere to the intima from the bloodstream and subsequently differentiate into macrophages. Within the intima, macrophages consume oxLDL to form large lipid-laden foam cells. The accumulation of foam cells produced by macrophages constitutes an early atherosclerotic plaque.

initial stage of atherosclerosis [48]. In this regard, Ibragimov et al. [35] developed a model of early atherosclerotic lesion formation by a system of non-linear partial differential equations (PDEs) where the concentration of oxLDL is expressed through a diffusion-reaction equation. Numerous studies on the early stage of atherosclerosis used diffusion-reaction transport model for oxLDL concentration [8] while some assume a constant transport [17]. The recruitment of monocytes from the lumen, their conversion to macrophages and finally, the production of foam cells from macrophages are necessary steps of plaque formation. Monocyte recruitment is initiated under the secretion of MCP-1 from the endothelium cells and differentiates into macrophages under the influence of M-CSF. Cilla et al. [15] introduced a convection-diffusion type PDE of oxLDL concentration that incorporates the production and degradation of MCP-1. In general, the secretion of MCP-1 can be coupled with the chemoattractant M-CSF [35, 24] as oxLDL is one of the critical factors behind atherosclerosis.

Monocyte recruitment and differentiation have been studied using simplified mathematical modelling where the governing equations describe the conversion of macrophages into foam cells after consuming oxLDL [8, 17, 11]. Ougrinovskaia et al. [50] develops a simplified model at an early stage, including the uptake of oxLDL by macrophages to form foam cells. Their model assumes Michaelis-Menten kinetics for the uptake of oxLDL by macrophages, and the recruitment of macrophages depends on oxLDL. Moreover, they have used a sigmoidal function for saturating the uptake rate. In the model of Cohen et al. [17], the effect of HDL in the early stage of atherosclerosis has been included. Nevertheless, the rest of the equations are the same as in Ougrinovskaia et al. [50]. El Khatib et al. [23, 21, 22] focus on plaque formation at an early stage of atherosclerosis where the density of monocytes and macrophages is represented as a system of reaction-diffusion equation. The presence of oxLDL draws monocytes or macrophages across the endothelium through nonlinear boundary conditions. A similar but more complicated model for early plaque formation has been proposed by Calvez et al. [8], which includes macrophages and oxLDL and a cytokine produced in response to the consumption of oxLDL by macrophages and prompts the recruitment of the monocyte at the endothelium. Calvez et al. [9] proposed an improved version of the previous model, coupled with a model for blood flow, to analyse how the distortion affects blood flow through the lumen region. Chalmers et al. [11] introduced a mathematical model of early atherosclerosis involving oxLDL, monocytes/macrophages, cytokines and foam cells to study the bifurcation analysis throughout the process.

Multiphase mixture theory has been widely used to model dynamic processes associated with biological tissues, remarkably heterogeneous tissues, for example, articular cartilage [47], solid tumor growth [7, 5] and scaffold growth in tissue engineering [40, 38]. Recently Watson et al. [55] have employed the mixture theory approach to model early fibrous cap formation and smooth muscle cells (SMCs) migration corresponding to the advanced stage of atherosclerosis plaque formation. The SMCs are a significant part of the plaque, and the remaining part may be regarded as non-SMC. Later, Watson et al. [56] considered the plaque tissue a mixture of three distinct phases: SMC phase, collagen-rich fibrous extracellular matrix (ECM) and a generic tissue phase comprising the remaining plaque constituents. In addition, their study considers collagen cap formation by SMCs in response to diffusible growth factors like PDGF and TGF- β from the endothelium. Consequently, multiphase models produce a detailed description of plaque formation dynamics since they provide a natural framework for volume exclusion and mechanical interaction between plaque constituents. In this study, a multiphase approach is deployed as both volume exclusion, and mechanical interaction can play a crucial role in the plaque growth of early atherosclerosis.

In most of the above studies, the plaque material has been considered advanced and stable without apprising its overall growth. Consequently, the interface between the intima and media remains static. Hence, early plaque growth prediction may not be possible through those models. On the other hand, many researchers believe that atherosclerosis is an obvious application of free boundary models, but for various reasons, most ignore it. Recently, Ahmed

et al. [1] developed a free boundary multiphase model corresponding to early atherosclerotic plaques to investigate the effects of impaired macrophage anti-inflammatory behaviour on plaque structure and its growth. The plaque is formed mainly by dead cells due to efferocytotic uptake by the macrophages. Motivated by the above developments of the atherosclerosis model, one can assume that the plaque boundary moves with a velocity equal to the speed of inflammatory tissue. The multiphase approach of the atherosclerosis model and moving plaque boundary can capture many mechanical and chemical features. For example, a tumor domain having free or moving boundary plays a significant role in the studies on tumor growth [5, 6]. This motivates us to investigate the model as free boundary domains in a systematic manner.

This paper is structured through several sections. In the next section, we formulate a mathematical model based on the mixture theory, assuming atherosclerotic plaque is a two-phase material composed of inflammatory and non-inflammatory tissues. Further, governing equations for the plaque growth are simplified for a 1D cartesian geometry. The governing equations are nonlinear due to the underlying physics; however, the Michaelis–Menten general kinetics corresponding to the oxLDL metabolism by macrophages is highly significant. In order to linearize the oxLDL transport equation, the perturbation expansion method is deployed by assuming the weak nonlinear nature of the oxLDL metabolism. Subsequently, the finite difference method is applied to the resulting leading and first-order equations satisfying the CFL condition. The novel feature of this study is the use of a combination of perturbation and numerical methods for efficiently handling the nonlinearity related to the oxLDL metabolism by macrophage.

2 Mathematical Formulation

We assume that the plaque grows by macrophages and foam cells for modelling an early-stage atherosclerotic plaque growth. Indeed the conversion of monocytes into macrophages and rapid oxidization of LDL inside the intima takes place on a much shorter time scale than the growth of the plaque [11]. Therefore, tracking monocytes within the intima at any instant would be difficult; hence, it is enough to consider a monocyte as a macrophage and oxLDL in place of LDL. At this stage, the plaque is supposed to consist of two distinct constituent phases. One consists of macrophages and foam cells; the other includes extracellular matrix, interstitial fluid, oxLDL, cytokines, and others. Since early atherosclerosis is an inflammatory disease involving mainly macrophages and macrophage-derived foam cells, one can name the first phase as the inflammatory cell phase. Therefore, the second phase is non-inflammatory. The migration and infiltration of inflammatory cells (monocytes or macrophages) are regulated by MCP-1, one of the key chemokines activated by the endothelium cells. MCP-1 and other cytokines (Endothelial Stimulating cytokines or ES cytokines etc.) responsible for the inflammatory cell phase migration can be regarded as functional cytokines (f-cytokines). Transport of oxLDL and f-cytokines are modelled using transport reaction equations.

We assume that the domain of the plaque region is $\Omega(t)$ in \mathbb{R}^d ($d = 1, 2, 3$) with a moving boundary. First, we define Γ_1 as a part of the plaque boundary corresponding to the lumen and intima interface, i.e., the endothelium. Next, we define $\Gamma_2(t)$ as the part of the boundary of $\Omega(t)$ corresponding to the IEL, which separates intima from media and that grows with time due to the deposition of macrophages and foam cells. Early plaque formation leads to compensatory expansion of an artery, during which the artery extends radially outward while preserving the lumen [37]. Consequently, the intima-IEL boundary $\Gamma_2(t)$ can be considered to vary over time. We introduce the index set \mathcal{C} containing the constituents of the plaque region. Note that \mathcal{C} is a finite set. In particular, assuming that the plaque is formed by the inflammatory cells (f) and non-inflammatory cells (n), we can consider $\mathcal{C} = \{f, n\}$. It also may be regarded as $\mathcal{C} = \{m, f, e\}$ where m stands for monocyte or macrophage, f stands for foam cell and e for extracellular fluid matrix in the plaque region. In this current study, we consider that the two different constituents form the plaque: inflammatory and non-inflammatory cells, i.e. $\mathcal{C} = \{f, n\}$. Instead, one can consider a multiphase model.

Define φ_i ($i \in \mathcal{C}$) as the volume fraction of each phase and \mathbf{v}_i ($i \in \mathcal{C}$) as the velocity of each phase. Also, let us denote \mathbb{T}_i ($i \in \mathcal{C}$) as the stress experienced by the i -th phase.

2.1 Mass Balance Equations

Assume that each phase has the same constant density. Mass balance equations corresponding to each phase can be expressed in the form

$$\frac{\partial \varphi_i}{\partial t} + \nabla \cdot (\varphi_i \mathbf{v}_i) = \mathbb{T}_i, \quad (i \in \mathcal{C}) \quad (1)$$

where $\mathbf{v}_i \in \mathbb{R}^d$ and $\mathbb{T}_i \in \mathbb{R}$ is the net source term corresponding to the i -th phase. Since the plaque is formed by the constituent of \mathcal{C} and there is no void, thus

$$\sum_{i \in \mathcal{C}} \varphi_i = 1. \quad (2)$$

The idea behind the plaque growth model is that after consuming oxLDL, macrophages transform into foam cells. Both the macrophages and foam cells are part of the inflammatory phase. Macrophages accumulate a vast amount of oxLDL, and at some point, gathered oxLDLs become toxic to foam cells [32]. Hence, the death of inflammatory cells, particularly foam cells, occurs, and the cellular debris becomes a part of the non-inflammatory phase. We assume the entire plaque development process forms a closed system, and there is no local source or sink of material. Therefore, the following satisfies

$$\sum_{i \in \mathcal{C}} \mathbb{T}_i = 0. \quad (3)$$

2.2 Momentum Balance Equations

Under no external force and negligible inertial effect, the momentum balance equations reduce to the balance equations between intraphase and interphase forces for each inflammatory and non-inflammatory phase:

$$\nabla \cdot (\varphi_i \mathbb{T}_i) + \mathbf{I}_i = 0, \quad (i \in \mathcal{C}) \quad (4)$$

where $\mathbb{T}_i \in \mathbb{R}^{d \times d}$ and $\mathbf{I}_i \in \mathbb{R}^d$ is the interphase force exerted on the i -th phase by the other phases. One may note that, according to Newton's third law of motion

$$\sum_{i \in \mathcal{C}} \mathbf{I}_i = 0. \quad (5)$$

In addition, we can simplify the above condition as follows, which is also consistent with the action-reaction principle:

$$\mathbf{I}_{i,j} = -\mathbf{I}_{j,i}, \quad \forall i, j \in \mathcal{C}, i \neq j \quad (6)$$

We assume the interphase force on the i -th constituent from the Darcy-like law by the following relations

$$\mathbf{I}_i = p \mathbb{I} \nabla \varphi_i + \sum_{j \in \mathcal{C}, j \neq i} \mathbf{K} \varphi_i \varphi_j (\mathbf{v}_j - \mathbf{v}_i) \quad (7)$$

in which, $p \in \mathbb{R}$ is the hydrodynamic pressure of the interstitial fluid. The second term on the right-hand side in equation (7) represents the relative velocity between the phases characterized by a typical drag coefficient $\mathbf{K} \in \mathbb{R}^{d \times d}$.

2.3 Mass Transport Equations

OxLDL and f-cytokines present within the non-inflammatory phase are governed by the pseudo-steady-state reaction-diffusion equations of the form

$$D_r \nabla \cdot (\varphi_n \nabla c_r) = Q_r, \quad r = \{1, 2\}, \quad (8)$$

in which c_1 and c_2 are concentrations of oxLDL and f-cytokines respectively. $D_r \in \mathbb{R}$ denotes the diffusion coefficient and $Q_r \in \mathbb{R}$ represents the net source or sink of the r -th species. Both Q_1 and Q_2 can be assumed to follow Michaelis-Menten kinetics. The convective transport of the above two species can be neglected without inertia due to the long transport time scale compared to diffusion.

2.4 Stress Components

We propose the following constitutive relations corresponding to the stresses \mathbb{T}_i ($i = n, f$) on the i -th constituent present in equation (4) [6, 55],

$$\mathbb{T}_f = -(p + \Sigma(\varphi_f) + \Lambda(c_2)) \mathbb{I}, \quad (9)$$

$$\mathbb{T}_n = -p\mathbb{I}, \quad (10)$$

where $\Sigma : [0, 1] \rightarrow \mathbb{R}$ is a nonlinear function of the volume fraction of the inflammatory phase φ_f ; $\Lambda : \mathbb{R} \rightarrow \mathbb{R}$ is another nonlinear function of the concentration of the f-cytokines c_2 ; \mathbb{I} is the identity tensor. For simplicity, viscous effects have been neglected in either phase. As the growth process continues, the increased volume of the foam cells induces a cell-cell interaction. Therefore, beyond a specific value of φ_f , the membrane of each cell starts to deform, and the cells experience stress. Correspondingly, Σ on the right-hand side of the equation (9) describes the pressure in the inflammatory phase due to that cell-cell interactions. The f-cytokines influence the migration of macrophages from the lumen to the intima. Consequently, one can assume the stress on the inflammatory phase is controlled by the concentration c_2 of f-cytokines, which is expressed through the function $\Lambda(c_2)$.

2.5 Initial and Boundary conditions

The following initial and boundary conditions are required to complete the model.

2.5.1 Initial Conditions:

Both the inflammatory phase volume fraction and the plaque outer boundary $\Gamma_2(t)$ are fixed initially:

$$\varphi_f(\mathbf{x}, 0) = \varphi_0, \quad \Gamma_2(t = 0) = \Gamma^0, \quad \text{for } \mathbf{x} \in \mathbb{R}^d. \quad (11)$$

2.5.2 Boundary Conditions:

On the interface of the endothelium and intima i.e. at the boundary Γ_1 , we suppose the zero-flux condition for inflammatory cells. Therefore, we set

$$(\mathbf{v}_f)|_{\Gamma_1} = (\mathbf{v}_n)|_{\Gamma_1} = 0. \quad (12)$$

The influx of LDL from the lumen into the intima occurs through the damaged portion of the endothelium. In the presence of free oxygen radicals inside the intima, LDL molecules oxidize to become oxLDL. The oxidization of LDL takes a much shorter time than plaque growth, as previously assumed. Consequently, both LDL influx and oxidation can be represented as a single process by the oxLDL influx. The flux of oxLDL through Γ_1 is assumed to be constant and given by [11],

$$(\nabla c_1 \cdot \hat{n})|_{\Gamma_1} = -\nu_1. \quad (13)$$

At the boundary Γ_1 , the flux of f-cytokines is modelled by

$$(\nabla c_2 \cdot \hat{n})|_{\Gamma_1} = -\nu_2 c_1 - \nu_3 c_2. \quad (14)$$

Chemokines produced at the endothelium in response to oxLDL constitute a family of chemoattractant cytokines that play a significant role in selectively recruiting monocytes etc. [43]. MCP-1, like chemokines produced at the endothelium, recruit monocytes, and the incident is expressed by the first term on the right-hand side of the equation (14). ES

cytokines enhance the production of MCP-1. As mentioned earlier, MCP-1, like chemokines and other ES cytokines, is regarded as f-cytokines. Therefore, in this context, it can be said that the production of f-cytokines by the endothelium depends on itself [11], which justifies the presence of the second term on the right-hand side of equation (14). Consequently, the flux of f-cytokines from the endothelium to the intima increases as the concentration of both oxLDL and f-cytokines increases at the endothelium [29].

On the moving plaque boundary $\Gamma_2(t)$, we assume continuity of stress so that total stress of inflammatory and non-inflammatory cell phase is same as the stress of the outer region which is supposed to be constant. We set

$$(\mathbb{T}_f + \mathbb{T}_n)|_{\Gamma_2(t)} = \mathbb{T}^{\text{con}}. \quad (15)$$

We also assume that outside the plaque boundary $\Gamma_2(t)$, oxLDL and f-cytokines concentration are constant, and thus we set

$$c_1|_{\Gamma_2(t)} = c_1^{\text{out}}, \quad (16)$$

$$c_2|_{\Gamma_2(t)} = c_2^{\text{out}}. \quad (17)$$

Finally, we assume that plaque moving boundary $\Gamma_2(t)$ expands at the same speed as the inflammatory cells on the boundary. Therefore, we define the following:

$$\frac{d\Gamma_2}{dt} = \mathbf{v}_f|_{\Gamma_2(t)}. \quad (18)$$

2.6 Constitutive Assumptions

2.6.1 Inflammatory Cell Phase Source Term

It is assumed that within the plaque, the inflammatory cell phase is produced from the non-inflammatory cell phase since the system is closed. Foam cells are produced when macrophages consume oxLDL, present in the non-inflammatory phase. Therefore, the birth of inflammatory cells depends on oxLDL concentration c_1 . On the other hand, the primary cause of inflammatory cell death is oxLDL-induced toxicity due to the excess concentration of c_1 . Therefore we choose Υ_f by assuming both birth and death saturating rates in following Michaelis-Menten kinetics:

$$\Upsilon_f = \underbrace{\varphi_f \varphi_n \frac{s_0 c_1}{1 + s_1 c_1}}_{\text{birth}} - \underbrace{\varphi_f \frac{s_2 + s_3 c_1}{1 + s_4 c_1} \mathcal{H}(c_1 - c_1^*)}_{\text{death}}, \quad (19)$$

where the first term corresponds to the production of inflammatory cells characterized by the parameters s_0 , s_1 , and the second one is the death of inflammatory cells characterized by s_2 , s_3 and s_4 . The production rate of inflammatory cells increases with c_1 up to a fixed value c_1^* (can be referred to as oxLDL-induced reference toxicity level), beyond which oxLDL results in the death of inflammatory cells. In other words, beyond such c_1^* , the death rate

of inflammatory cells increases with c_1 . \mathcal{H} in equation (19) denotes the Heaviside function which can be approximated by a smooth function as

$$\mathcal{H}(x, \epsilon) = \frac{1}{2} \left(1 + \tanh \frac{x}{\epsilon} \right), \quad \epsilon \ll 1. \quad (20)$$

2.6.2 OxLDL and f-Cytokines Source Terms

Net source or sink of oxLDL Q_1 can be assumed as follows

$$Q_1 = \underbrace{\varphi_f \varphi_n \frac{q_0 c_1}{1 + q_1 c_1}}_{\text{consumption}} - \underbrace{\varphi_f \varphi_n q_2 c_1}_{\text{release}}, \quad (21)$$

in which q_0 , q_1 and q_2 are positive constants. The first term on the right side describes the loss of oxLDL due to the oxLDL consumption by macrophages to become foam cells. We use a Michaelis-Menten general kinetics type function to represent it. The oxLDL released by the dead foam cells are assumed to obey a constant decay rate (see the second term on the right-hand side of equation (21)) [3]. Note that there may be a loss of oxLDL, perhaps through degradation, but we do not include this for simplicity.

Similarly, Q_2 can be set as

$$Q_2 = \underbrace{\varphi_n q_3 c_2}_{\text{decay}} - \underbrace{\varphi_n \varphi_f q_4 c_1 c_2}_{\text{production}}, \quad (22)$$

where q_3 and q_4 are positive constants. Cytokines secreted from foam cells in presence of oxLDL [10]. Correspondingly, the production of f-cytokines depends on φ_f and c_1 , as shown by the second term of the right hand side of above equation. The first term represents a linear decay in c_2 .

2.6.3 Terms Contributing on Stress Tensors

The function Σ in equation (9) represents the pressure on inflammatory cell phase due to cell-cell interactions, which can be expressed as

$$\Sigma(\varphi_f) = \frac{\varphi_f - \varphi^*}{(1 - \varphi_f)^2} \mathcal{H}(\varphi_f - \varphi^*), \quad (23)$$

where \mathcal{H} is the Heaviside function and φ^* is the volume fraction of foam cells and macrophages beyond which cells experience stress. Our choice of Σ follows the study of Beward et al. [5], Byrne et al. [7], etc. f-Cytokines act as chemoattractants to pull monocytes from the lumen into the intima. It has already been mentioned that monocytes rapidly transform into macrophages inside the intima. Hence, the movement of macrophages within the intima can be assumed to be influenced by f-cytokines concentration (i.e. chemotaxis). Therefore, Λ in equation (9) can be defined to be

$$\Lambda = \frac{\chi}{1 + (\kappa c_2)^m}, \quad (24)$$

where χ , κ and m are positive parameters. The assumption implies that the stress from the inflammatory phase decreases with increasing f-cytokines concentration, allowing the chemoattractant to move. Correspondingly, it is represented as a mechanism of stress relief in the inflammatory cell phase [55]. The chemotactic function Λ also can be defined as $\chi/(1 + \kappa c_2)^2$, but in the case of the receptor binding, it may be more reasonable to describe by Hill function as shown in (24) [33]. In this model, monocytes enter the intima from the bloodstream with the help of receptors VCAM-1 and ICAM-1. Consequently, our study would prefer to consider the chemotaxis function as (24).

3 One-Dimensional Model

As the first step, we study plaque growth in one dimension along the x -axis. It occupies the region $0 \leq x \leq l(t)$ (see Figure 2). Consequently, the boundary Γ_1 reduces to $x = 0$ (i.e., the interface of the endothelium and intima), and the moving edge $\Gamma_2(t)$ corresponding to the interface of the intima and IEL is now $x = l(t)$, which is the width of the growing plaque at time t in the early stage. This one-dimensional model would enable us to focus on the cellular and biochemical mechanisms without worrying about the geometry of the domain. In addition, the diameter of an artery is significantly larger than the width of the intima at the early stages of plaque formation [4], which makes it reasonable to use Cartesian coordinates as an approximation for radial coordinates. We denote all the physical variables consistent with the previous section. The above scenario compels us to reduce the mass balance equations (1) into the following form:

$$\frac{\partial \varphi_f}{\partial t} + \frac{\partial}{\partial x} (\varphi_f v_f) = \Upsilon_f, \quad (25)$$

$$\frac{\partial \varphi_n}{\partial t} + \frac{\partial}{\partial x} (\varphi_n v_n) = \Upsilon_n. \quad (26)$$

Similarly, the momentum conservation equations (4) reduces as,

$$\frac{\partial}{\partial x} (\varphi_f T_f) + I_f = 0, \quad (27)$$

$$\frac{\partial}{\partial x} (\varphi_n T_n) + I_n = 0, \quad (28)$$

in which

$$I_f = p \frac{\partial \varphi_f}{\partial x} + k \varphi_f \varphi_n (v_n - v_f) \quad (29)$$

and

$$I_n = p \frac{\partial \varphi_n}{\partial x} + k \varphi_f \varphi_n (v_f - v_n), \quad (30)$$

as obtained from (7). The stresses described in equations (9) and (10) are reduced into the following 1D form as

$$T_f = -p - \Sigma(\varphi_f) - \Lambda(c_2) \quad (31)$$

and

$$T_n = -p \quad (32)$$

respectively.

Next, the mass transport equations (8) are reduced as follows

$$D_1 \frac{\partial}{\partial x} \left(\varphi_n \frac{\partial c_1}{\partial x} \right) = Q_1, \quad (33)$$

$$D_2 \frac{\partial}{\partial x} \left(\varphi_n \frac{\partial c_2}{\partial x} \right) = Q_2. \quad (34)$$

Finally, The initial and boundary conditions (11)-(18) become

$$\varphi_f = \varphi_0, \quad l = l_0, \quad \text{at } t = 0 \quad (35)$$

$$v_f = v_n = 0, \quad \text{at } x = 0 \quad (36)$$

$$D_1 \frac{\partial c_1}{\partial x} = -\nu_1, \quad \text{at } x = 0 \quad (37)$$

$$D_2 \frac{\partial c_2}{\partial x} = -\nu_2 c_1 - \nu_3 c_2, \quad \text{at } x = 0 \quad (38)$$

$$T_f + T_n = T^{\text{con}}, \quad \text{at } x = l(t) \quad (39)$$

$$c_1 = c_1^{\text{out}}, \quad \text{at } x = l(t) \quad (40)$$

$$c_2 = c_2^{\text{out}}, \quad \text{at } x = l(t) \quad (41)$$

and

$$\frac{dl}{dt} = v_f. \quad \text{at } x = l(t) \quad (42)$$

4 Model Simplification

In this section, we reduce the model into a system of nonlinear partial differential equations in φ_f , v_f , c_1 and c_2 that describe the plaque growth at the early stage. The model simplification is quite similar to that of Breward et al. [5], Watson et al. [55], and for clarity, the model simplification is included in detail.

We add the mass balance equations (25) and (26), to get

$$\frac{\partial}{\partial x} (\varphi_f v_f + \varphi_n v_n) = 0 \quad (43)$$

which on imposing the zero-flux boundary condition (36) at the endothelium and intima interface (i.e. $v_f = v_n = 0$ at $x = 0$), the velocity of non-inflammatory cell phase v_n can be expressed in terms of the velocity of inflammatory cells v_f in the following way:

$$v_n = -\frac{\varphi_f}{\varphi_n} v_f \quad (44)$$

Similarly, summing the momentum balance equations (27) and (28), and submitting the stress expressions T_f and T_n from (31)-(32), we find the following equation

$$\frac{\partial p}{\partial x} + \frac{\partial F_1}{\partial x} = 0 \quad (45)$$

where F_1 has the following expression

$$F_1 = \varphi_f \Sigma + \varphi_f \Lambda \quad (46)$$

From (45), with the help of (27), (29) and (31), we derive the following:

$$\varphi_n \frac{\partial F_1}{\partial x} + k \varphi_f v_f = 0 \quad (47)$$

Consequently, using the mass balance equation (25), we deduce

$$\frac{\partial \varphi_f}{\partial t} - \frac{\varphi_n}{k} \frac{\partial^2 F_1}{\partial x^2} - \frac{1}{k} \frac{\partial \varphi_n}{\partial x} \frac{\partial F_1}{\partial x} = \Upsilon_f \quad (48)$$

Therefore, our reduced model can be read as the equation (48) coupled with equations (47), (33) and (34) subject to the initial and boundary conditions prescribed by (35)-(42).

4.1 Nondimensionalization

Using hat ($\hat{\cdot}$) to denote dimensionless quantities, we scale the independent and dependent variables x , t , l , v_f , c_1 , c_2 , φ_f and φ_n , as follows (one can note that, inflammatory and non-inflammatory cell phase volume fractions φ_f and φ_n respectively do not require scaling):

$$\hat{x} = x/l_0, \quad \hat{t} = t/(kl_0^2/T^{\text{con}}), \quad \hat{l} = l/l_0, \quad \hat{v}_f = v_f/(T^{\text{con}}/kl_0).$$

$$\hat{c}_1 = c_1/c_1^{\text{out}}, \quad \hat{c}_2 = c_2/c_2^{\text{out}}, \quad \hat{\varphi}_f = \varphi_f, \quad \hat{\varphi}_n = \varphi_n.$$

We introduced the non-dimensional parameters in the following way:

$$\hat{\Upsilon}_f = \Upsilon_f/(T^{\text{con}}/kl_0^2), \quad \hat{\Sigma} = \Sigma/T^{\text{con}}, \quad \hat{\Lambda} = \Lambda/T^{\text{con}}, \quad \hat{T}_f = T_f/T^{\text{con}},$$

$$\hat{T}_n = T_n/T^{\text{con}}, \quad \hat{F}_1 = F_1/T^{\text{con}}, \quad \hat{Q}_1 = Q_1/(D_1 c_1^{\text{out}}/l_0^2), \quad \hat{Q}_2 = Q_2/(D_2 c_2^{\text{out}}/l_0^2),$$

$$\hat{\nu}_1 = \nu_1/(D_1 c_1^{\text{out}}/l_0), \quad \hat{\nu}_2 = \nu_2/(D_2 c_2^{\text{out}}/l_0 c_1^{\text{out}}), \quad \hat{\nu}_3 = \nu_3/(1/l_0).$$

The corresponding model equations, initial and boundary conditions in non-dimensional form reduces to

$$\frac{\partial \hat{\varphi}_f}{\partial \hat{t}} - \hat{\varphi}_n \frac{\partial^2 \hat{F}_1}{\partial \hat{x}^2} - \frac{\partial \hat{\varphi}_n}{\partial \hat{x}} \frac{\partial \hat{F}_1}{\partial \hat{x}} = \hat{\Upsilon}_f \quad (49)$$

$$\hat{\varphi}_n \frac{\partial \hat{F}_1}{\partial \hat{x}} + \hat{\varphi}_f \hat{\nu}_f = 0 \quad (50)$$

$$\frac{\partial}{\partial \hat{x}} \left(\hat{\varphi}_n \frac{\partial \hat{c}_1}{\partial \hat{x}} \right) = \hat{Q}_1, \quad (51)$$

$$\frac{\partial}{\partial \hat{x}} \left(\hat{\varphi}_n \frac{\partial \hat{c}_2}{\partial \hat{x}} \right) = \hat{Q}_2. \quad (52)$$

$$\hat{\varphi}_f = \varphi_0, \quad \hat{l} = 1, \quad \text{at } \hat{t} = 0 \quad (53)$$

$$\hat{v}_f = \hat{v}_n = 0, \quad \text{at } \hat{x} = 0 \quad (54)$$

$$\frac{\partial \hat{c}_1}{\partial \hat{x}} = -\hat{\nu}_1, \quad \text{at } \hat{x} = 0 \quad (55)$$

$$\frac{\partial \hat{c}_2}{\partial \hat{x}} = -\hat{\nu}_2 \hat{c}_1 - \hat{\nu}_3 \hat{c}_2, \quad \text{at } \hat{x} = 0 \quad (56)$$

$$\hat{T}_f + \hat{T}_n = 1, \quad \text{at } \hat{x} = \hat{l}(t) \quad (57)$$

$$\hat{c}_1 = 1, \quad \text{at } \hat{x} = \hat{l}(t) \quad (58)$$

$$\hat{c}_2 = 1, \quad \text{at } \hat{x} = \hat{l}(t) \quad (59)$$

and

$$\frac{d\hat{l}}{d\hat{t}} = \hat{v}_f. \quad \text{at } \hat{x} = \hat{l}(t). \quad (60)$$

Without loss of generality, we drop the hat ('^') from the model field equations, and initial and boundary conditions unless otherwise stated explicitly.

4.2 Simplifying Boundary Conditions

Before going through the numerical solutions, it can be useful to simplify the boundary conditions (54) and (57) in order to generate simulations.

From the zero-flux boundary condition of inflammatory cells (54) at $x = 0$, we obtain

$$v_f = v_n = 0, \quad (61)$$

and with the help of equation (50), it can be obtained at $x = 0$ that

$$\frac{\partial}{\partial x} (\varphi_f \Lambda) = -\frac{\partial}{\partial x} (\varphi_f \Sigma). \quad (62)$$

We assume that at the interface of the endothelium and intima (i.e. at $x = 0$), inflammatory cells do not interact with each other so that

$$\frac{\partial}{\partial x} (\varphi_f \Lambda) = 0, \quad \text{at } x = 0. \quad (63)$$

Similarly from the stress boundary condition equation (57), at $x = l(t)$ we have

$$T_f + T_n = 1, \quad (64)$$

which further reduces to at $x = l(t)$:

$$\Sigma + \Lambda = -2p - 1. \quad (65)$$

At the plaque boundary $x = l(t)$, we assume the interstitial hydrodynamic pressure (p) in such a way that $2p + 1 = 0$. We therefore have

$$\Sigma(\varphi_f) = -\Lambda(c_2) \quad \text{at } x = l(t). \quad (66)$$

4.3 Change of Variables

In order to execute numerical solutions, it is convenient to map the moving domain onto a fixed one. Consequently, we change the variable (x, t) to (ζ, τ) by the transformation $\zeta = x/l(t)$ and $\tau = t$. The transformed problem reduces to

$$\frac{\partial \varphi_f}{\partial \tau} - \frac{\zeta}{l} \frac{dl}{d\tau} \frac{\partial \varphi_f}{\partial \zeta} - \frac{\varphi_n}{l^2} \frac{\partial^2 F_1}{\partial \zeta^2} - \frac{1}{l^2} \frac{\partial \varphi_n}{\partial \zeta} \frac{\partial F_1}{\partial \zeta} = \nabla_f, \quad (67)$$

$$\varphi_n \frac{\partial F_1}{\partial \zeta} + l \varphi_f v_f = 0, \quad (68)$$

$$\frac{\partial}{\partial \zeta} \left(\varphi_n \frac{\partial c_1}{\partial \zeta} \right) = l^2 Q_1, \quad (69)$$

$$\frac{\partial}{\partial \zeta} \left(\varphi_n \frac{\partial c_2}{\partial \zeta} \right) = l^2 Q_2, \quad (70)$$

with initial and boundary conditions

$$\varphi_f = \varphi_0, \quad l = 1, \quad \text{at } \tau = 0 \quad (71)$$

$$\frac{\partial}{\partial \zeta} (\varphi_f \Lambda) = 0, \quad \text{at } \zeta = 0 \quad (72)$$

$$\frac{\partial c_1}{\partial \zeta} = -l\nu_1, \quad \text{at } \zeta = 0 \quad (73)$$

$$\frac{\partial c_2}{\partial \zeta} = -l\nu_2 c_1 - l\nu_3 c_2, \quad \text{at } \zeta = 0 \quad (74)$$

$$\Sigma(\varphi_f) = -\Lambda(c_2), \quad \text{at } \zeta = 1 \quad (75)$$

$$c_1 = 1, \quad \text{at } \zeta = 1 \quad (76)$$

$$c_2 = 1, \quad \text{at } \zeta = 1 \quad (77)$$

and

$$\frac{dl}{d\tau} = v_f \quad \text{at } \zeta = 1. \quad (78)$$

5 Computational Technique

We employ a stable finite difference scheme for the numerical solution of the governing equations. Specifically, explicit finite difference methods are applied to solve parabolic-type partial differential equations. The present differential nonlinear system is parabolic and amenable to using explicit finite-difference formulation. The forward-time central space (FTCS) method is an explicit finite-difference scheme, and correspondingly, in this study, we used the FTCS scheme to solve the problem. This method has been used in several studies to solve governing equations numerically [58, 2, 39] and the details about convergence and stability are available in the book of Hoffmann and Chiang [34]. This scheme approximates spatial derivatives by central difference formulae, while the forward difference formula approximates the time derivative.

We discrete the region (0,1) into N equal cells of size $\Delta\zeta = 1/N + 1$ with a time step $\Delta\tau > 0$. Define $\zeta_j = (j - 1)\Delta\zeta$, $j = 1, 2, \dots, N + 1$, and $\tau_n = (n - 1)\Delta\tau$, $n = 1, 2, \dots$, and approximations $(\varphi_f)_j^n = \varphi_f(\zeta_j, \tau_n)$, $(c_1)_j^n = c_1(\zeta_j, \tau_n)$, and $(c_2)_j^n = c_2(\zeta_j, \tau_n)$. Spatial and time derivative approximations are as follows:

$$\frac{\partial c_\ell}{\partial \zeta} \cong \frac{(c_\ell)_{j+1}^n - (c_\ell)_{j-1}^n}{2\Delta\zeta}, \quad \ell = 1, 2 \quad (79)$$

$$\frac{\partial^2 c_\ell}{\partial \zeta^2} \cong \frac{(c_\ell)_{j+1}^n - 2(c_\ell)_j^n + (c_\ell)_{j-1}^n}{(\Delta\zeta)^2}, \quad \ell = 1, 2 \quad (80)$$

$$\frac{\partial \varphi_f}{\partial \zeta} \cong \frac{(\varphi_f)_{j+1}^n - (\varphi_f)_{j-1}^n}{2\Delta\zeta}, \quad (81)$$

$$\frac{\partial^2 \varphi_f}{\partial \zeta^2} \cong \frac{(\varphi_f)_{j+1}^n - 2(\varphi_f)_j^n + (\varphi_f)_{j-1}^n}{(\Delta\zeta)^2}, \quad (82)$$

and

$$\frac{\partial \varphi_f}{\partial \tau} \cong \frac{(\varphi_f)_j^{n+1} - (\varphi_f)_j^n}{\Delta\tau}. \quad (83)$$

The system (67)-(78) is discretized based on the approximations (79)-(83) and solved. We start with a given $(\varphi_f)_j^n$ to compute $(c_1)_j^n$, $(c_2)_j^n$ using which $(\varphi_f)_j^{n+1}$ is evaluated. We have taken $N = 30$ spatial steps and 10^5 time steps to satisfy the CFL condition of the explicit scheme and obtain the accuracy of the order $\sim 10^{-7}$.

In equation (69), the term Q_1 is nonlinear in c_1 . Applying the central difference formula (79)-(80) in (69), a system of nonlinear equations in $(c_1)_1^n, (c_1)_2^n, \dots, (c_1)_{N+1}^n$ when $q_1 \neq 0$ is obtained. Newton's method can solve this nonlinear system, which is a meticulous job requiring high numerical programming skills. As a result, some studies assume $q_1 = 0$ to remove the nonlinearity [5, 39]. But, this restricts the general kinetics and reduces it to first-order kinetics, a particular case of Michaelis–Menten kinetics. In the present study, we deal with the general kinetics and consider q_1 as a small parameter ($q_1 \ll 1$) so that

it becomes a perturbation parameter rather than taking the vanishing limit. Therefore, we reduce the nonlinear form of Q_1 in the variable c_1 to a weakly linearized form using perturbation approximation with the perturbed parameter q_1 as described in the following section.

5.1 Perturbation Approximations

We consider the following perturbation approximations

$$c_\ell = c_\ell^{(0)} + q_1 c_\ell^{(1)} + \mathcal{O}(q_1^2), \quad \ell = 1, 2 \quad (84)$$

$$\varphi_f = \varphi_f^{(0)} + q_1 \varphi_f^{(1)} + \mathcal{O}(q_1^2), \quad (85)$$

$$v_f = v_f^{(0)} + q_1 v_f^{(1)} + \mathcal{O}(q_1^2). \quad (86)$$

Using the above approximations, we can get the following expansions

$$\varphi_n = \varphi_n^{(0)} + q_1 \varphi_n^{(1)} + \mathcal{O}(q_1^2), \quad (87)$$

$$\Upsilon = \Upsilon^{(0)} + q_1 \Upsilon^{(1)} + \mathcal{O}(q_1^2), \quad (88)$$

$$\Sigma = \Sigma^{(0)} + q_1 \Sigma^{(1)} + \mathcal{O}(q_1^2), \quad (89)$$

$$\Lambda = \Lambda^{(0)} + q_1 \Lambda^{(1)} + \mathcal{O}(q_1^2), \quad (90)$$

$$F_1 = F_1^{(0)} + q_1 F_1^{(1)} + \mathcal{O}(q_1^2), \quad (91)$$

and

$$Q_\ell = Q_\ell^{(0)} + q_1 Q_\ell^{(1)} + \mathcal{O}(q_1^2), \quad \ell = 1, 2 \quad (92)$$

where the expressions of $\varphi_n^{(0)}$, $\varphi_n^{(1)}$, $\Upsilon^{(0)}$, $\Upsilon^{(1)}$, $\Sigma^{(0)}$, $\Sigma^{(1)}$, $\Lambda^{(0)}$, $\Lambda^{(1)}$, $F_1^{(0)}$, $F_1^{(1)}$, $Q_1^{(0)}$, $Q_1^{(1)}$, $Q_2^{(0)}$, and $Q_2^{(1)}$ are described in the Appendix A and B. Correspondingly, the leading and $\mathcal{O}(q_1)$ problems reduce as shown in the following sections.

5.1.1 The Leading Order Problem

The governing equations corresponding to leading order problem reduce to

$$\frac{\partial \varphi_f^{(0)}}{\partial \tau} - \frac{\zeta}{l} \frac{dl}{d\tau} \frac{\partial \varphi_f^{(0)}}{\partial \zeta} - \frac{\varphi_n^{(0)}}{l^2} \frac{\partial^2 F_1^{(0)}}{\partial \zeta^2} - \frac{1}{l^2} \frac{\partial \varphi_n^{(0)}}{\partial \zeta} \frac{\partial F_1^{(0)}}{\partial \zeta} = \Upsilon_f^{(0)}, \quad (93)$$

$$\varphi_n^{(0)} \frac{\partial F_1^{(0)}}{\partial \zeta} + l \varphi_f^{(0)} v_f^{(0)} = 0 \quad (94)$$

$$\frac{\partial}{\partial \zeta} \left(\varphi_n^{(0)} \frac{\partial c_1^{(0)}}{\partial \zeta} \right) = l^2 Q_1^{(0)}, \quad (95)$$

$$\frac{\partial}{\partial \zeta} \left(\varphi_n^{(0)} \frac{\partial c_2^{(0)}}{\partial \zeta} \right) = l^2 Q_2^{(0)}, \quad (96)$$

with initial and boundary conditions

$$\varphi_f^{(0)} = \varphi_0, \quad l = 1, \quad \text{at } \tau = 0 \quad (97)$$

$$\frac{\partial}{\partial \zeta} \left(\varphi_f^{(0)} \Lambda^{(0)} \right) = 0 \quad \text{at } \zeta = 0 \quad (98)$$

$$\frac{\partial c_1^{(0)}}{\partial \zeta} = -l\nu_1, \quad \text{at } \zeta = 0 \quad (99)$$

$$\frac{\partial c_2^{(0)}}{\partial \zeta} = -l\nu_2 c_1^{(0)} - l\nu_3 c_2^{(0)}, \quad \text{at } \zeta = 0 \quad (100)$$

$$\Sigma^{(0)} \left(\varphi_f^{(0)} \right) = -\Lambda^{(0)} \left(c_2^{(0)} \right), \quad \text{at } \zeta = 1 \quad (101)$$

$$c_1^{(0)} = 1, \quad \text{at } \zeta = 1 \quad (102)$$

$$c_2^{(0)} = 1, \quad \text{at } \zeta = 1 \quad (103)$$

and

$$\frac{dl}{d\tau} = v_f^{(0)} \quad \text{at } \zeta = 1. \quad (104)$$

5.1.2 The $\mathcal{O}(q_1)$ Problem

In first order, the governing equations reduce as

$$\frac{\partial \varphi_f^{(1)}}{\partial \tau} - \frac{\zeta}{l} \frac{dl}{d\tau} \frac{\partial \varphi_f^{(1)}}{\partial \zeta} - \frac{\varphi_n^{(0)}}{l^2} \frac{\partial^2 F_1^{(1)}}{\partial \zeta^2} - \frac{\varphi_n^{(1)}}{l^2} \frac{\partial^2 F_1^{(0)}}{\partial \zeta^2} - \frac{1}{l^2} \frac{\partial \varphi_n^{(0)}}{\partial \zeta} \frac{\partial F_1^{(1)}}{\partial \zeta} - \frac{1}{l^2} \frac{\partial \varphi_n^{(1)}}{\partial \zeta} \frac{\partial F_1^{(0)}}{\partial \zeta} = \Upsilon_f^{(1)}, \quad (105)$$

$$\varphi_n^{(0)} \frac{\partial F_1^{(1)}}{\partial \zeta} + \varphi_n^{(1)} \frac{\partial F_1^{(0)}}{\partial \zeta} + l\varphi_f^{(0)} v_f^{(1)} + l\varphi_f^{(1)} v_f^{(0)} = 0 \quad (106)$$

$$\frac{\partial}{\partial \zeta} \left(\varphi_n^{(0)} \frac{\partial c_1^{(1)}}{\partial \zeta} + \varphi_n^{(1)} \frac{\partial c_1^{(0)}}{\partial \zeta} \right) = l^2 Q_1^{(1)}, \quad (107)$$

$$\frac{\partial}{\partial \zeta} \left(\varphi_n^{(0)} \frac{\partial c_2^{(1)}}{\partial \zeta} + \varphi_n^{(1)} \frac{\partial c_2^{(0)}}{\partial \zeta} \right) = l^2 Q_2^{(1)}, \quad (108)$$

with the initial and boundary conditions

$$\varphi_f^{(1)} = 0, \quad l = 1, \quad \text{at } \tau = 0 \quad (109)$$

$$\frac{\partial}{\partial \zeta} \left(\varphi_f^{(0)} \Lambda^{(1)} + \varphi_f^{(1)} \Lambda^{(0)} \right) = 0 \quad \text{at } \zeta = 0 \quad (110)$$

$$\frac{\partial c_1^{(1)}}{\partial \zeta} = 0, \quad \text{at } \zeta = 0 \quad (111)$$

$$\frac{\partial c_2^{(1)}}{\partial \zeta} = -\nu_2 c_1^{(1)} - \nu_3 c_2^{(1)}, \quad \text{at } \zeta = 0 \quad (112)$$

$$\Sigma^{(1)} \left(\varphi_f^{(1)} \right) = -\Lambda^{(1)} \left(c_2^{(1)} \right), \quad \text{at } \zeta = 1 \quad (113)$$

$$c_1^{(1)} = 0, \quad \text{at } \zeta = 1 \quad (114)$$

$$c_2^{(1)} = 0. \quad \text{at } \zeta = 1 \quad (115)$$

Now, the terms $Q_1^{(0)}$ and $Q_1^{(1)}$ are both linear in $c_1^{(0)}$ and $c_1^{(1)}$ respectively (see Appendix A & B). Therefore, in order to compute $c_1^{(0)}$ and $c_1^{(1)}$ numerically from the equations (95) and (107), we can apply central difference formulae (79)-(80). Correspondingly, we will get a system of linear equations for each case, and can be solved using Thomas algorithm. Then we compute $c_2^{(0)}$, $c_2^{(1)}$ in a similar way and finally we evaluate $\varphi_f^{(0)}$ and $\varphi_f^{(1)}$. Consequently, we numerically obtain the solution of the leading and $\mathcal{O}(q_1)$ problem. Hence, the complete solution is determined upto $\mathcal{O}(q_1)$ from the equations (84)-(86).

6 Numerical Simulations

In this section, we systematically analyze the numerical results on the oxidized LDL concentration, volume of inflammatory phase (foam cells + macrophages), concentration of f-cytokines responsible for macrophage migration, the variation of plaque width over time, etc. First, we set the values of parameters of interest. Subsequently, numerical simulations are performed.

6.1 Model Parameterisations

The mechanism of plaque formation in atherosclerosis is slow enough. Therefore, the time scale for the simulation is considered in days. As mentioned by Hao and Friedman [31], the diffusion coefficients for oxidized LDL and f-cytokines (in particular for MCP-1) are $29.89 \text{ cm}^2 \text{ day}^{-1}$ and $17.28 \text{ cm}^2 \text{ day}^{-1}$ respectively. q_0 represents the rate of metabolism of oxidized LDL by macrophages, which is 10^4 day^{-1} [45]. Similarly, the study of Cobbold et al. [16] suggests the value of q_2 (the rate of oxLDL production) as $2.35 \times 10^{-7} \text{ day}^{-1}$. In addition, Hao and Friedman [31] and Chen et al. [14] respectively support the production and decay rates of f-cytokines (i.e., q_4 and q_3) as $0.96 \times 10^{10} \text{ g}^{-1} \text{ cm}^3 \text{ day}^{-1}$ and 1.73 day^{-1} . As reported by Hao and Friedman [31], within the intima, the concentration of oxLDL and f-cytokines are $7 \times 10^{-4} - 1.9 \times 10^{-3} \text{ g cm}^{-3}$ and $3 \times 10^{-10} \text{ g cm}^{-3}$ respectively. The chemotactic sensitivity parameter χ , as mentioned in equation (24) can be set as $15.5 \times 10^{-16} \text{ g cm}^{-1} \text{ day}^{-2}$ [36]. Further, the clinical study of Grootaert et al. [26] mentions a standard intimal width as $75 \mu\text{m}$. Since the early plaque growth is restricted within the intima, one can choose the initial plaque width as 10^{-2} cm . With the data set mentioned above, we calculate the corresponding non-dimensional values of the parameters q_0 , q_2 , q_3 , q_4 and χ as listed in Table 1. In addition, this table contains the calculated dimensionless values of constants ν_1 , ν_2 and ν_3

Parameter	Dimensionless value	Supporting literature
q_0	3.3×10^{-1}	McKay et al. [45]
q_2	7.8×10^{-14}	Cobbold et al. [16]
q_3	1×10^{-6}	Chen et al. [14]
q_4	5×10^{-1}	Hao and Friedman [31]
χ	1×10^{-1}	Kim and Friedman [36]
κ	1×10^{-1}	—
m	2	—
l_0	10^{-2}	Grootaert et al. [26]
ν_1	$10^{-2} - 10^1$	Chalmers et al. [11]
ν_2	$10^{-2} - 10^1$	Ougrinovskaia et al. [50]
ν_3	$10^{-3} - 10^1$	Chalmers et al. [11]

Table 1: Calculated dimensionless values of the parameters from the mentioned literatures.

Parameter	Value
s_0	3×10^{-1}
s_1	10
s_2	10^{-3}
s_3	10^{-1}
s_4	10

Table 2: Estimated values of the non-dimensional parameters contributing in inflammatory phase source term

that are present in equations (73)-(74) from the studies of Chalmers et al. [11], Ougrinovskaia et al. [50].

It is seen that there needs to be more literature to provide precise values for the non-dimensional parameters κ and m present in the chemotactic function Λ . As a result, suitable estimates for these parameters would be much handy. In this regard, the behaviour of Λ against c_2 is shown in Figure 3a to estimate κ and m . Now following Hillen and Painter [33], we may choose the value of the parameters within the ranges of $0 < \kappa < 1$ and $1 < m < 3$. The chemotactic function generally has a decreasing nature corresponding to all values within the ranges, as shown in Figure 3a. Λ is plotted for three different values of $\kappa = 0.05, 0.1, 0.2$ and $m = 1.5, 2, 2.5$. It is observed from Figure 3a that for higher values of κ , the chemotactic function decays faster; however, this decay is slow for large m . Therefore, $\kappa = 0.1$ and $m = 2$ could be a worthy choice.

Similarly, we go through the behaviour of the inflammatory phase net source Υ_f that appears in equation (19) to estimate the value of the parameters s_0, s_1, s_2, s_3 and s_4 (shown in the Figure 3b). s_0 and s_1 are decided inversely proportional to each other such that the first part (birth term) of Υ_f , which grows with c_1 , justifies inflammatory phase growth. We consider

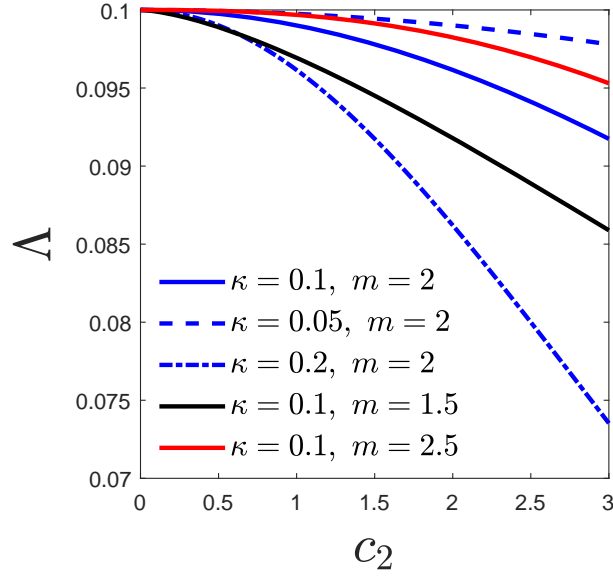
that the death of the inflammatory phase occurs due to the toxicity of oxLDL, where c_1^* is the reference toxicity level. Consequently, the contribution of the death term (i.e. second part in Υ_f) in the inflammatory cell production increases with c_1 for values higher than c_1^* . Therefore, throughout the study, $s_2 < s_3/s_4$ can be assumed. In addition, s_3 and s_4 may behave inversely towards the increasing nature of the death term. Hence upon the choice of s_4 within $[1, 10]$, it may be suitable to consider s_3 in $[0.1, 1]$ with the assumption $s_2 < s_3/s_4$. Also, the literature suggests that when $s_1 = s_4 = 0$ (first-order kinetics), the parameters s_0 and s_3 lies in the range $0.1 \leq s_0, s_3 \leq 10$ [51, 20]. In order to fix the value of the parameters within the above ranges, we may refer to Figure 3b. Note that when $s_0 \leq s_3$, the net source term becomes negative, as shown by the blue dotted and dash-dotted lines. This incident may be physically unrealistic as the inflammatory phase forms the plaque. Hence, we can consider $s_0 > s_3$ with $s_0 = 0.3, s_3 = 0.1$. In addition, in each of the following cases, $s_1 < s_4$, $s_1 = s_4$ and $s_1 > s_4$, the corresponding scenarios are shown by the solid red, blue and black curves, respectively. Similar arguments are valid for the case $s_1 \leq s_4$. For simplicity, we choose $s_1 = s_4 = 10$ following the study of Breward et al. [5] on tumor growth. Finally, the value of the parameter s_2 is considered as 10^{-3} to satisfy the condition $s_2 < s_3/s_4$. The above-estimated parameter values are prescribed in Table 2.

6.2 Results and Discussion

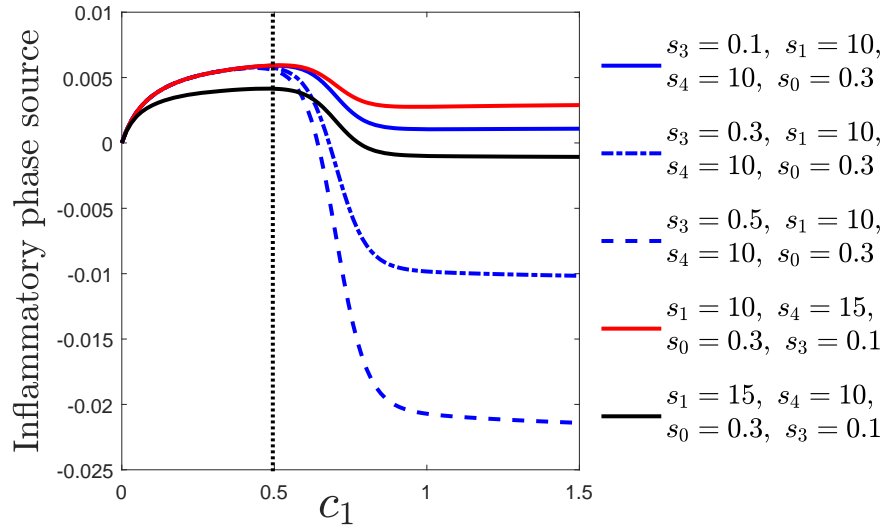
The distributions of inflammatory cell volume fraction, oxLDL and f-cytokines concentration are illustrated through Figures 4a-4c respectively for various times with fixed $\varphi_f^0 = 0.6$, $\varphi^* = 0.4$, $c_1^* = 0.5$ and other parameters from Tables 1 and 2. The parameters φ_f^0 and φ^* are chosen so that cell-cell interactions are initially included and continued at these values unless otherwise stated. It is observed from Figure 4a that inflammatory cells accumulate predominantly towards the endothelium-intima interface (i.e. $x = 0$).

As both oxLDL and f-cytokines are secreted from the endothelium, their concentrations are high at that interface and decrease away from it (Figures 4b-4c). The time evolution of these model variables is presented for $t = 10, 20, 25, 30$. With time, the inflammatory cell population increases throughout the intima (Figure 4a). Due to the uptake of oxLDL by macrophages, the increasing density of inflammatory cells reduces oxLDL concentration with time (Figure 4b). However, the f-cytokines diffusion increases with increasing t (Figure 4c). It is because of f-cytokines secretion from the inflammatory cells. The density of inflammatory cells increases with time, resulting in enhanced f-cytokine concentration. Figure 4d represents the change in plaque width with time. It shows that initially, the growth is exponential, but after a certain period, the growth rate decreases, and the process becomes stable. In other words, the speed with which the moving edge proceeds remains almost constant after an initial period. The pressure on the plaque from its surroundings within the intima may inhibit plaque growth. In addition, the toxicity of oxLDL may affect the growth process, and the details are discussed in the consequent sections.

Within intima, macrophages consume oxLDL to become lipid-laden foam cells, and both



(a)



(b)

Figure 3: Variation of (a) Chemotactic function Λ with respect to c_2 , (b) Inflammatory phase source Υ_f with c_1 corresponding to various parameters described in the figures.

macrophages and foam cells co-exist at the inflammatory cell phase. Consequently, inflammatory cell volume fraction depends on oxLDL concentration. Although the cause of macrophage and foam cell death within the intima has not been studied immoderately, a few studies suggest that the toxicity of oxLDL is responsible for the death [32, 44, 42]. Hence, we consider inflammatory cell death due to the toxicity of oxLDL with the toxicity level c_1^* described in equation (19). Figure 5a depicts the variation of inflammatory cell volume fraction with oxLDL concentration corresponding to $c_1^* = 1.05$ (oxLDL induced reference

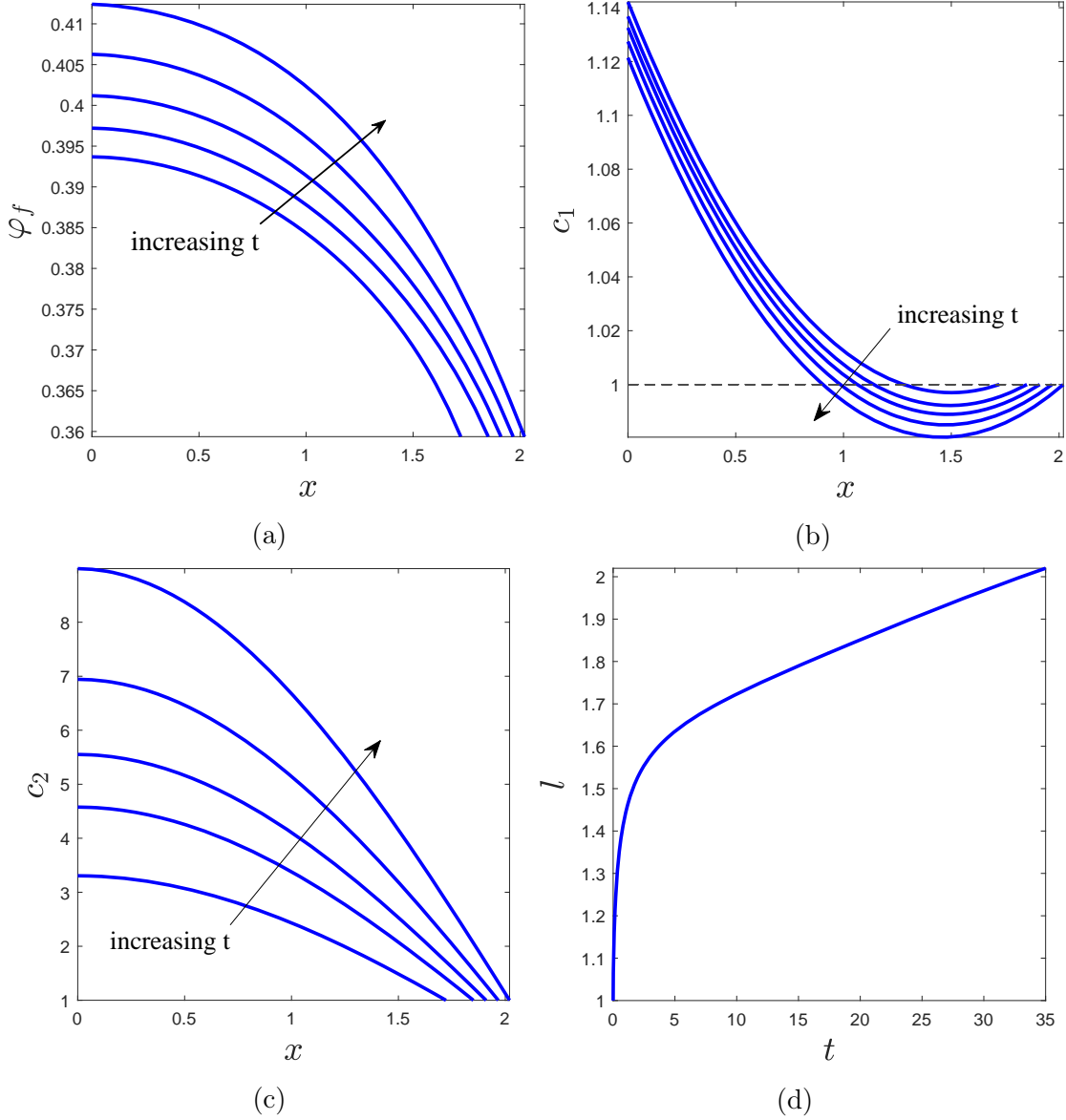


Figure 4: (a) Inflammatory cell volume fraction, (b) OxLDL concentration, and (c) f-Cytokines (MCP-1) concentration distributions in the intima at an early stage of atherosclerosis plaque formation for various $t_{\text{fix}} = 10, 20, 25, 30$ and 35 . The direction of these sequential time points is indicated by the arrows. (d) Graph shows the evolution of plaque width $l(t)$ with t .

toxicity level) at various times. Accordingly, we choose $t = t_{\text{fix}}$ where $t_{\text{fix}} = 10, 15, 20, 25$ etc. Corresponding to each t_{fix} , one can identify φ_f and c_1 as the function of $x(t = t_{\text{fix}})$ such that for each $t = t_{\text{fix}}$ we get both the values of φ_f and c_1 at each point of the plaque. Evidently, the data-set $(c_1, \varphi_f) = (1, 0.36)$ corresponds to the plaque boundary. Initially, the inflammatory cell population increases with c_1 as the consumption of oxLDL produces them.

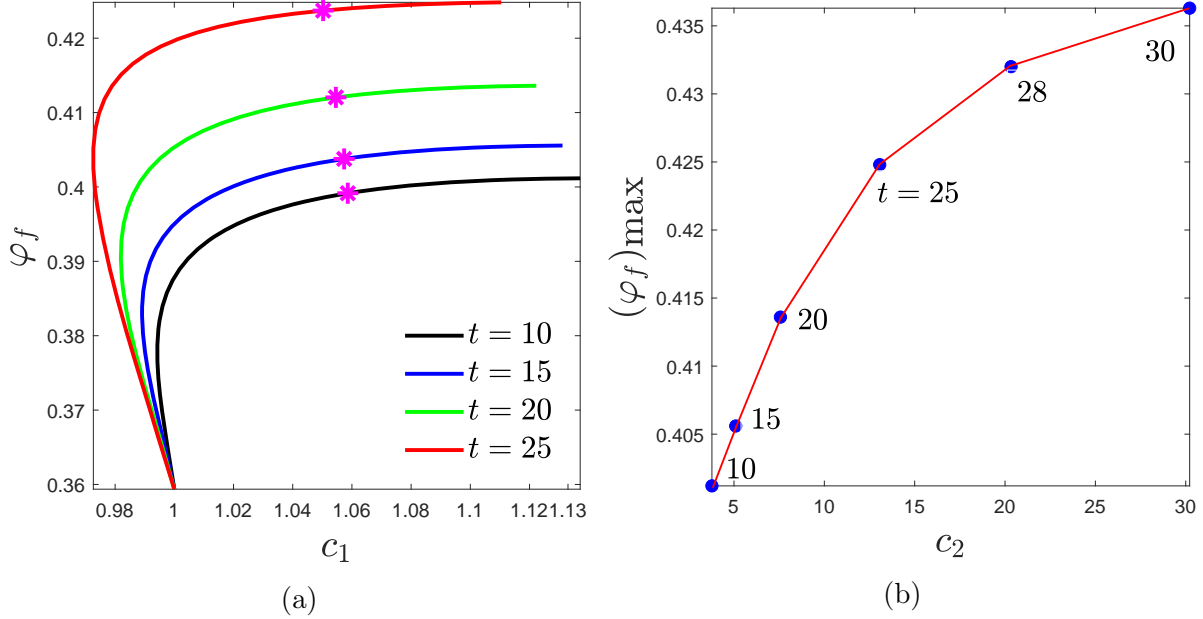


Figure 5: (a) Inflammatory cell volume fraction variation with oxLDL concentration, (b) Maximum volume fraction of inflammatory cells at different times with respect to f-cytokines concentration. The star markers in (a) indicate the volume fraction of inflammatory cells corresponding to $c_1^* = 1.05$, and the blue dots in (b) represent the maximum value corresponding to $t = 10, 15, 20, 25, 28, 30$.

Subsequently, the death of inflammatory cells starts due to c_1 exceeding c_1^* . Consequently, the increasing nature of φ_f ceases, and it saturates to a nearly constant value (Figure 5a). Moreover, this figure enables us to detect two different values of φ_f corresponding to $c_1 = 1$ for each $t = t_{\text{fix}}$. The occurrence of two different values of φ_f corresponding to the same c_1 (in particular, the magnitude of c_1 at the plaque moving boundary) takes place due to the triggering of oxLDL induced toxicity. This may be due to the same concentration of oxLDL at two different points within the plaque. Later, we will discuss this issue in the following section through Figure 6.

In response to the f-cytokines, monocytes or macrophages enter the intima and form foam cells. Consequently, f-cytokines concentration influences the production of inflammatory cells. In Figure 5b, we show the locus of maximum growth of inflammatory cells $((\varphi_f)_{\max})$ against f-cytokines at different times (each blue dot represents value for the corresponding time that is indicated). The maximum growth of inflammatory cells is expected to reach a steady state. In the next section, we discuss the impact of oxLDL and f-cytokines influx parameters in plaque development.

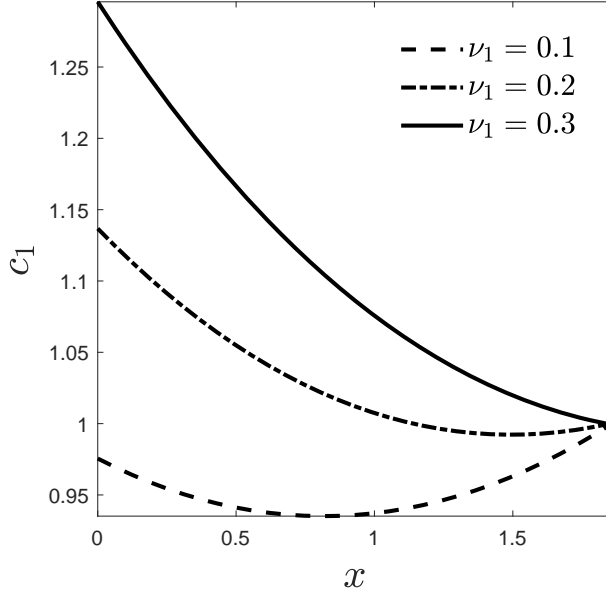


Figure 6: Variation of the oxLDL concentration for different ν_1 .

6.2.1 The Roll of oxLDL and f-Cytokines Influxes ν_1 , ν_2 and ν_3 on the Plaque Growth Behaviour

LDL molecules from the bloodstream enter the intima through the damaged endothelium and are oxidized to become oxLDL. As the oxidization process happens concisely, in this long-timescale study, it is convenient to assume the influx of oxLDL through the endothelium from the lumen to the intima. The parameter ν_1 represents oxLDL flux into the intima and can be considered proportional to the blood LDL cholesterol level [11]. The level of f-cytokines controls the macrophage migration into the intima and the parameters ν_2 , ν_3 correspond to the f-cytokines influx. In addition, the flux of f-cytokines is enhanced due to oxLDL concentration through ν_2 and f-cytokines itself via ν_3 .

Figure 6 displays the oxLDL concentration profile corresponding to different flux rates ν_1 . One can notice that for the larger value of ν_1 , the concentration of oxLDL increases throughout the intima. Consequently, it may impact f-cytokine concentration, inflammatory cell population, and plaque growth, which we shall discuss in the following sections. However, Figure 6 illustrates an interesting fact. For $\nu_1 = 0.3$, c_1 shows a decreasing nature within the plaque with the maximum value at $x = 0$. On the other hand, for $\nu_1 = 0.1$, we have the same magnitude of c_1 to occur at two different locations within the plaque with $c_1(x = 0) < c_1(x = l(t_{\text{fix}}))$. This is because, corresponding to $\nu_1 = 0.3$, the production of oxLDL at the endothelium-intima interface is much higher than any other location within the intima. On the other hand, such production of oxLDL is less in the case of $\nu_1 = 0.1$. In this situation, at any locations within the intima, $c_1(x) > c_1(x = 0) \forall x \in (0, l(t))$. At those locations, the death of foam cells occurs due to oxLDL-induced toxicity and as a

consequence, an increase in c_1 results from the release of excess oxLDL from dead foam cells.

The effect of the influxes ν_1 , ν_2 and ν_3 on the f-cytokines concentration are depicted through Figures 7a-7c respectively. It is seen that the concentration of f-cytokines within intima grows with the value for all the influx indices. The secretion of f-cytokines at the endothelium is influenced by oxLDL which in turn show a monotonic behavior with the influx index ν_1 (see Figure 6). Consequently, f-cytokines concentration increases with ν_1 as shown in Figure 7a. In addition, increasing ν_2 and ν_3 induces f-cytokines influx at the endothelium. As a result, f-cytokines concentration within the intima increased with ν_2 (Figure 7b) and ν_3 (Figure 7c).

Oxidized LDL (oxLDL) enriches the production of f-cytokines at the endothelium and the secretion is characterised by ν_2 . The f-cytokines profile in Figure 8 indicates the increasing nature initially and then decreases to a steady state. After a certain level, oxLDL becomes toxic to inflammatory cells as well as f-cytokines. Consequently, the increasing nature of f-cytokines reduces to the steady state. Increasing ν_2 results more f-cytokines within intima (see Figure 8), which is consistent with the earlier result (Figure 7b). Moreover, it can be observed that the level after which decay of f-cytokines begins due to oxLDL toxicity increases for larger ν_2 . These results suggest that the toxicity of oxLDL has a significant effect on f-cytokines concentration and increased f-cytokines secretion from the endothelium enhances the level of f-cytokines degradation.

The influence of ν_1 , ν_2 and ν_3 on the population of inflammatory cells are shown through the Figures 9a-9c respectively. As seen in Figures 6, 7b and 7c, the concentration of oxLDL as well as f-cytokines is enhanced with the increasing influx parameters. In response to the f-cytokines, more macrophages migrate into the intima and consume oxLDL to become foam cells. Consequently, the volume of inflammatory cells gets enhanced with the influx parameters.

Early plaque development depends on the inflammatory cell phase in the presence of oxLDL and f-cytokines, as was earlier noted. Consequently, the plaque width is controlled by ν_1 , ν_2 and ν_3 , which is depicted through Figures 10a-10c. In particular, Figure 10a illustrates an interesting feature. Initially, the growth of the curves corresponding to $\nu_1 = 0.1$ (black solid), $\nu_1 = 0.5$ (dot-dashed), and $\nu_1 = 0.8$ (dot) are very similar, and subsequently, variations follow. Higher ν_1 leads to producing more oxLDL within the intima. Beyond a high threshold concentration of oxLDL within the intima, oxLDL becomes toxic to inflammatory cells. Due to the elevated level of toxicity, the solid curve is noticeably beneath the dot-dashed curve beyond a threshold distance, where the dashed curve grows quicker than the dot-dashed curve. Therefore, the plaque growth rate reduces with higher oxLDL flux ν_1 . On the other hand, a notable impact of f-cytokines within intima is experienced at the larger magnitude of ν_2 and ν_3 that consequences a high concentration of f-cytokines. Consequently, inflammatory response causes more macrophages to migrate at the intima under the influence of increased f-cytokines, resulting in an increased macrophage population. Hence, the proliferation of new foam cells has resulted within intima to reinforce early plaque growth. Consequently, early

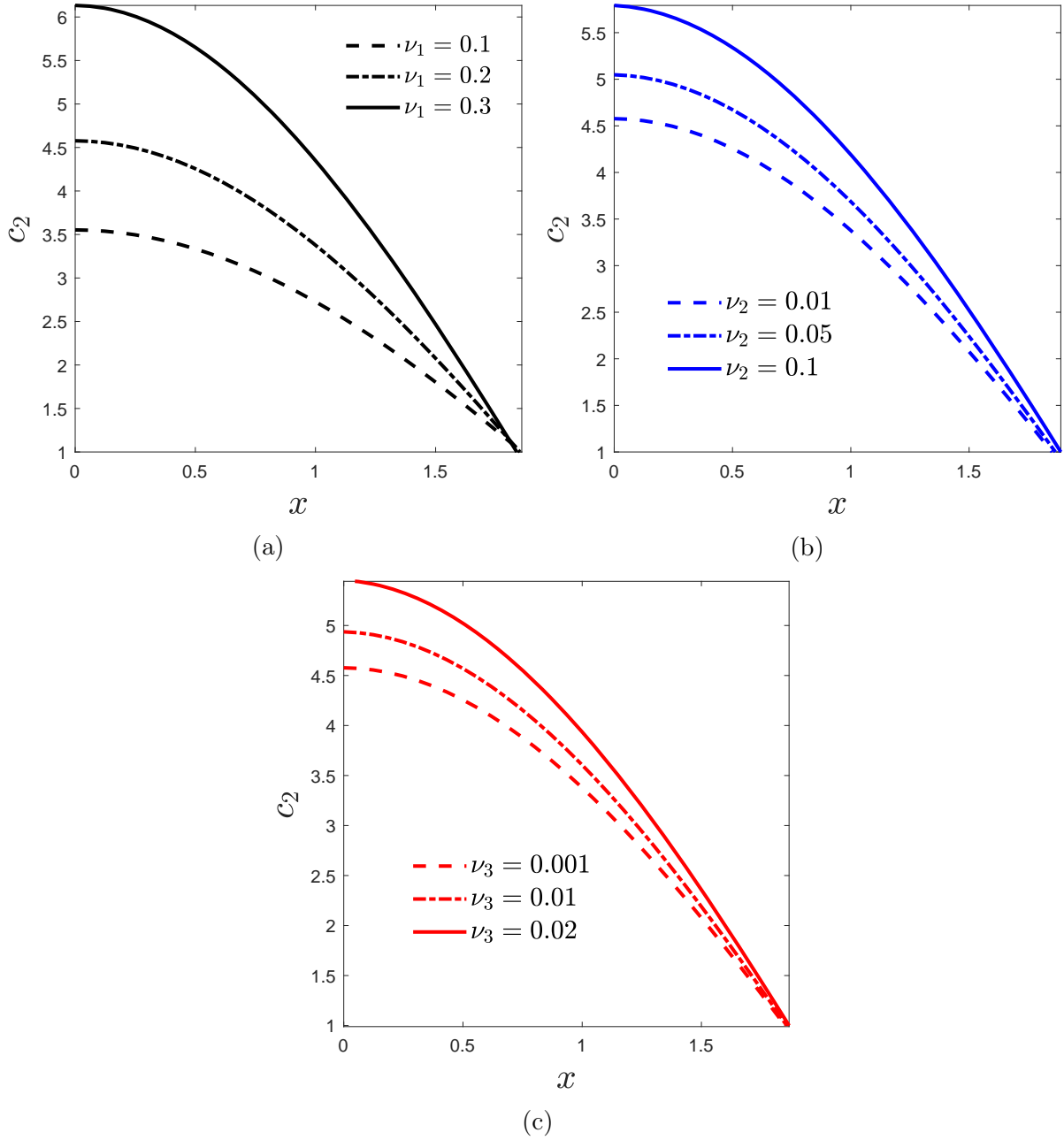


Figure 7: Distribution of f-cytokines concentration for various (a) ν_1 , (b) ν_2 and (c) ν_3 .

plaque growth is positively correlated with the values of ν_2 (Figure 10b) and ν_3 (Figure 10c). Therefore, ν_2 and ν_3 are productive while ν_1 is counterproductive towards the inflammatory response of the entire plaque development.

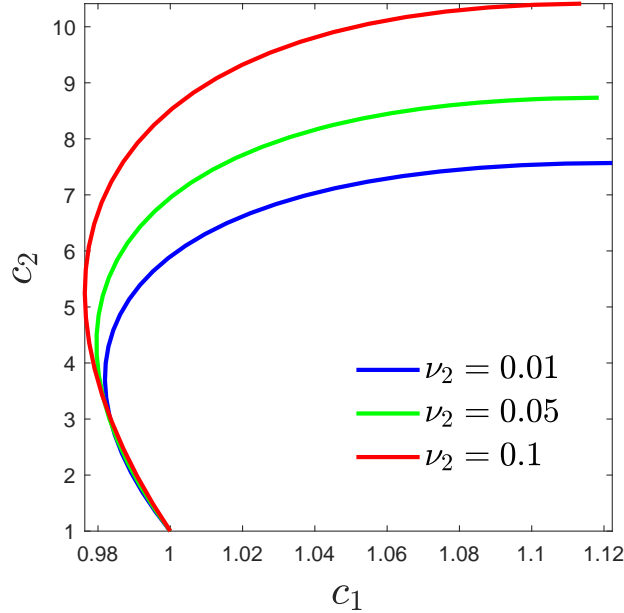


Figure 8: Variation of f-cytokines concentration with oxLDL concentration corresponding to different ν_1 .

6.2.2 Effect of Initial Volume of Inflammatory Cells (φ_f^0) and Toxicity Level Corresponding to oxLDL (c_1^*)

In order to study the early growth of plaque, an input initial volume of inflammatory cells (φ_f^0) is needed. Accordingly, we illustrate the impact of φ_f^0 on φ_f , c_1 , c_2 , $l(t)$ through Figures 11a-11d respectively. At a fixed cross section, the population of inflammatory cells increases with φ_f^0 (see Figures 11a). If we compare the difference in φ_f growth from $\varphi_f^0 = 0.55$ to 0.60 and the corresponding one from 0.60 to 0.65, we see that the deviation is most prominent at the endothelium-intima interface and becomes negligible towards the plaque periphery. Such variations can be observed due to the impact of φ_f^0 on the oxLDL and f-cytokines concentrations. In this context, let us examine the impact of φ_f^0 on c_1 through Figure 11b which depicts that φ_f^0 mathematically reciprocates with the concentration of oxLDL i.e., c_1 . This behaviour seems to oppose the result illustrated in Figure 5a. Besides the recruitment of oxLDL through damaged endothelium into the intima, oxLDLs are produced in the form of release from dead foam cells (see equation 21). Increasing φ_f^0 leads to the production of more inflammatory cells that can consume excess oxLDL. Thus, each foam cell experiences less toxicity at higher φ_f^0 . Consequently, the death rate of foam cells reduces, and that causes less production of oxLDL from inflammatory cells (foam cells). This enables us to understand how c_1 mathematically reciprocates with φ_f^0 . On the contrary, the behaviour of φ_f^0 on c_2 is found to behave inversely with that of c_1 (see Figure 11c). Since the inflammatory cells release f-cytokines to cause an additional inflammatory response of recruiting new monocytes into the intima [52, 10] and higher φ_f^0 develops more inflammatory cells, so c_2 increases with φ_f^0 as illustrated through Figure 11c. Besides, it is already noticed that higher φ_f^0 reinforces

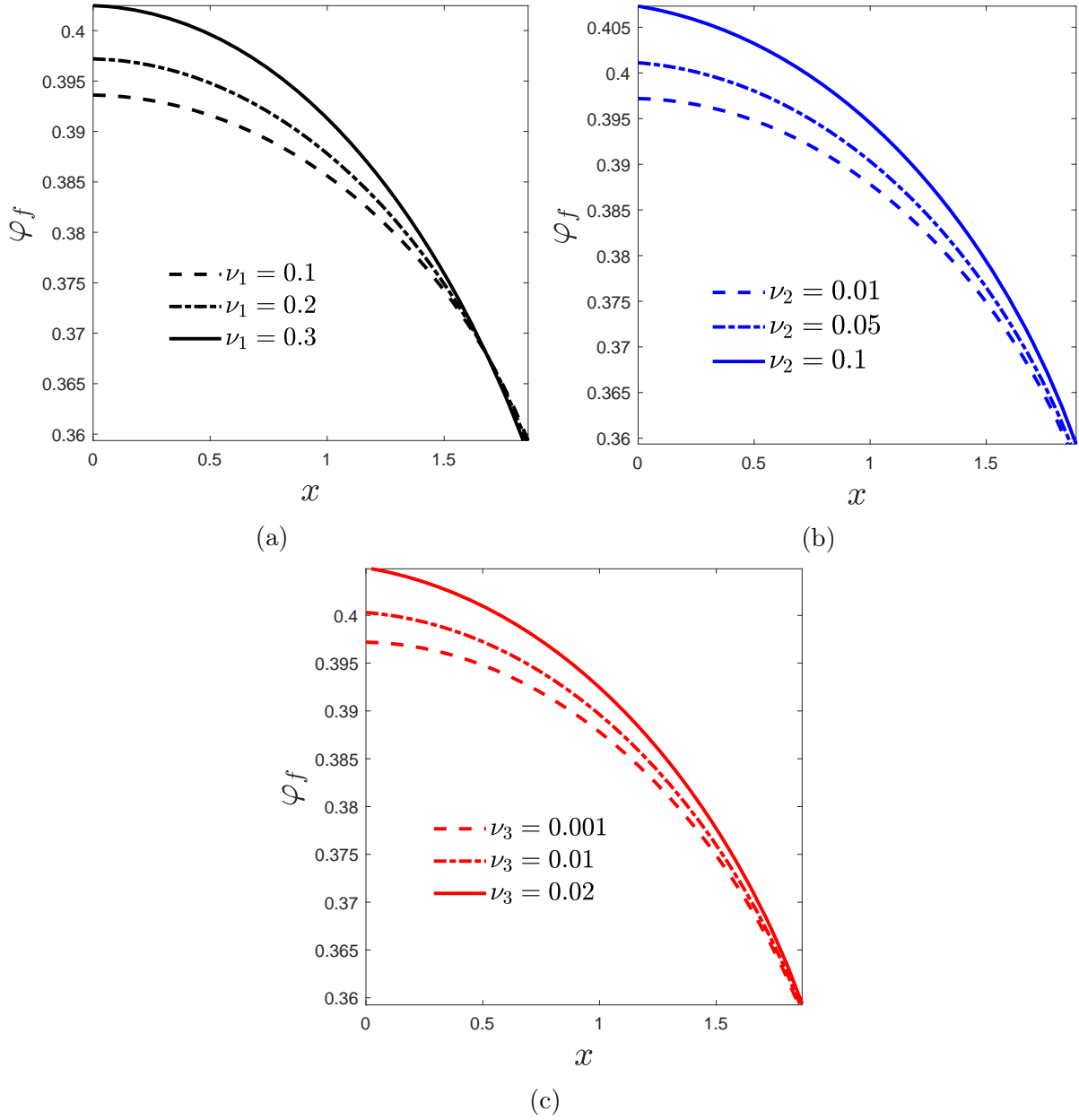


Figure 9: Variation of Inflammatory cell volume fraction for different (a) ν_1 , (b) ν_2 , and (c) ν_3 .

the inflammatory process by generating more inflammatory cells (see Figure 11a). In this context, Figure 11d depicts the influence of φ_f^0 on the plaque width growth, which shows that φ_f^0 is found to accelerate the plaque width. Consequently, the plaque formed by the inflammatory cells, grows more rapidly with increasing φ_f^0 .

As mentioned earlier, the toxicity induced by oxLDL causes inflammatory cell death. Con-

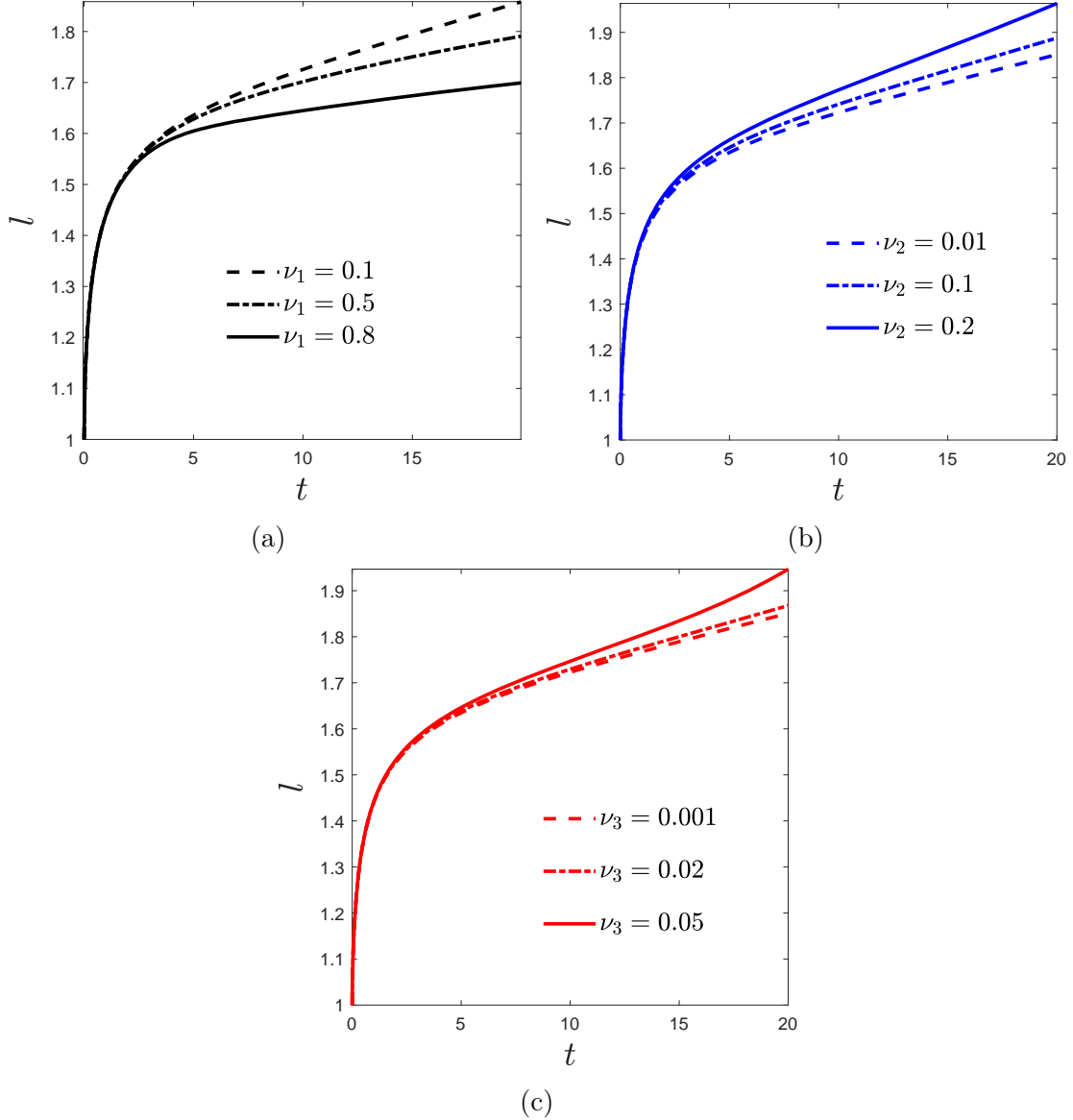


Figure 10: Profiles of plaque width growth for various (a) ν_1 , (b) ν_2 , and (c) ν_3 .

sequently, variation in the toxicity level c_1^* can have a significant contribution to plaque formation. The results for the different toxicity levels c_1^* on inflammatory cell volume and plaque width growth are shown through Figures 12a-12b respectively. Both these variables are impacted by different toxicity levels. As previously stated, inflammatory cells start to die when oxLDL reaches its toxicity level. The higher toxicity level signifies more inflammatory cell development than the lower level due to the proliferation and absence of death up to that level. Consequently, the volume fraction of inflammatory cells increases as c_1^* rises (Figure 12a). Furthermore, as depicted in Figure 12b, an increase in c_1^* results in an increase in plaque width growth. Corresponding to a larger c_1^* , the population of inflammatory cells

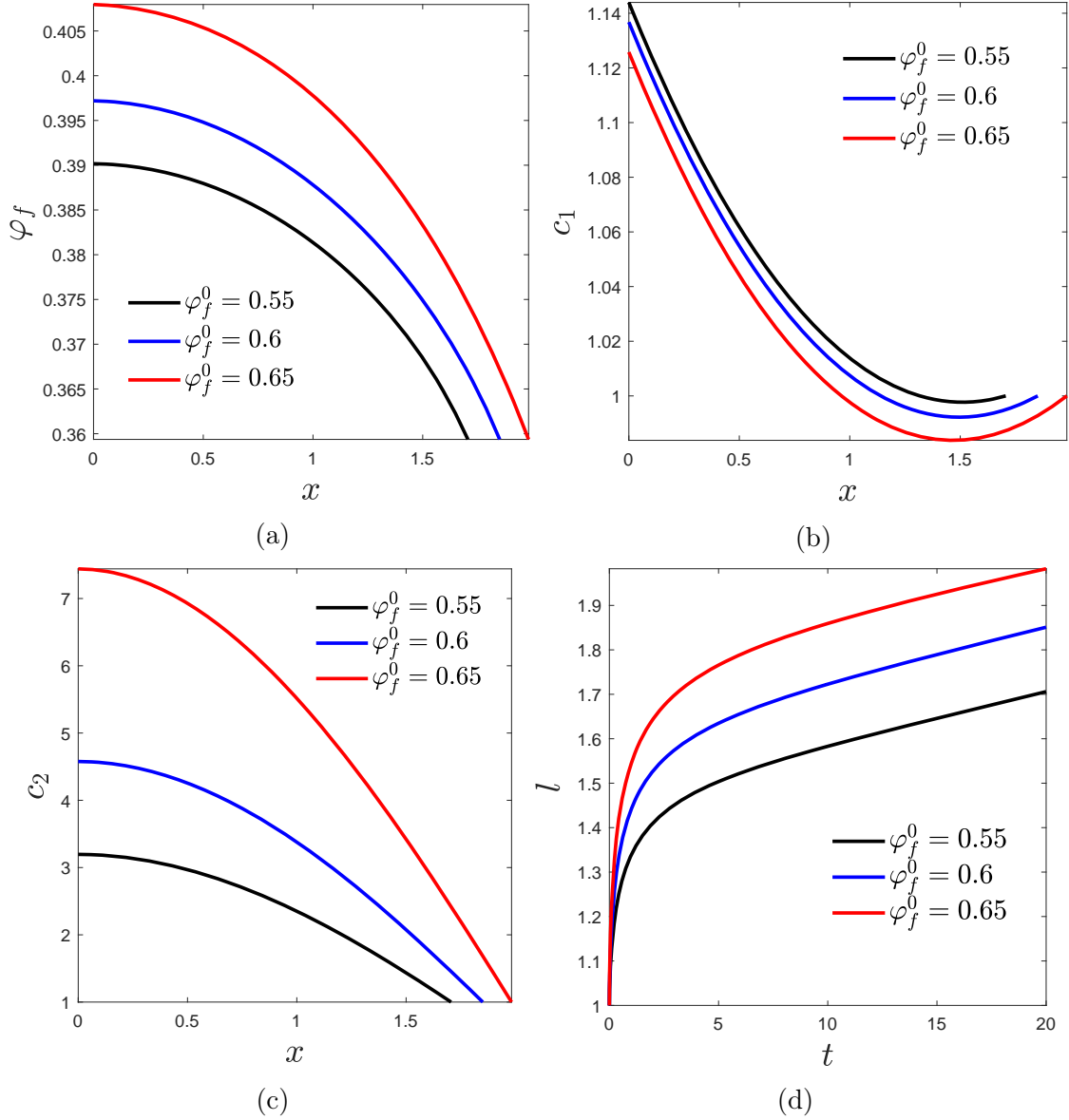


Figure 11: Variations of (a) Inflammatory cell volume fraction, (b) oxLDL concentration, (c) f-Cytokines concentration with x , and (d) Plaque width growth with t for different φ_f^0 .

increases. As a result, the growth of the plaque, formed by the deposition of inflammatory cells, accelerates with the increased c_1^* .

6.3 Qualitative Agreement with the Clinical Studies

We made an attempt to compare some of the results from this study with existing clinical studies done by Meyer et al. [46] and Stangeby and Ethier [54]. Accordingly, the LDL concentrations within the arterial intima are picked up from these studies corresponding to

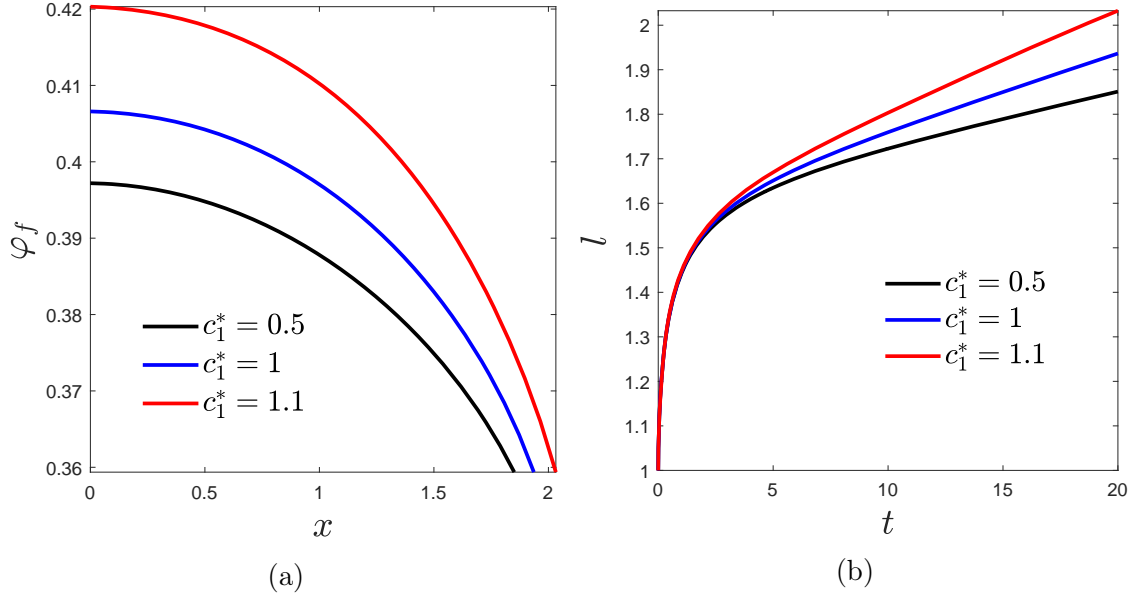


Figure 12: (a) Distributions of Inflammatory cell volume fraction, and (d) Plaque width growth with t within the intima corresponding to various c_1^* .

transmural pressures of $p = 70, 120, 160$ mmHg. The LDL concentration data are extracted using the grabit toolbox of MATLAB R2021a, are normalized first before comparing with the oxLDL concentrations obtained from the present study at each point within the intima. The process of the normalization is done in such a way that the domain of clinical data maps onto that of the present study through a suitable transformation. Such transformation enables us to focus much on the qualitative agreement rather than quantitative. Note that the present study is focused on oxLDL rather than LDL as the oxidization takes place in a short time while growth is a long time scale process. Figures 13a and 13b delineate the above mentioned comparative study. In the first figure, the oxLDL (present study) and LDL (Stangeby and Ethier [54]) concentrations are plotted corresponding to $\nu_1 = 0.2, 0.3$ and $p = 120, 160$, respectively. In the next figure, a similar comparison is made between the present study and Meyer et al. [46] corresponding to $\nu_1 = 0.1, 0.2, 0.3$ and $p = 70, 120, 160$ respectively. A good qualitative agreement between the clinical and present studies has been observed, and the comparisons show that the normalized LDL (obtained from Meyer et al. [46] and Stangeby and Ethier [54]) and oxLDL (obtained from the current study) concentrations behave similarly. Both are highly concentrated in the vicinity of the lumen or endothelium-intima interface and decrease toward the media or arterial wall.

7 Summary and Conclusions

The role of macrophages and foam cells has been studied at an early stage of atherosclerosis. Based on the multiphase mixture theory, we develop a mathematical model that introduces oxLDL-induced toxicity over plaque growth in early atherosclerosis. Foam cell death oc-

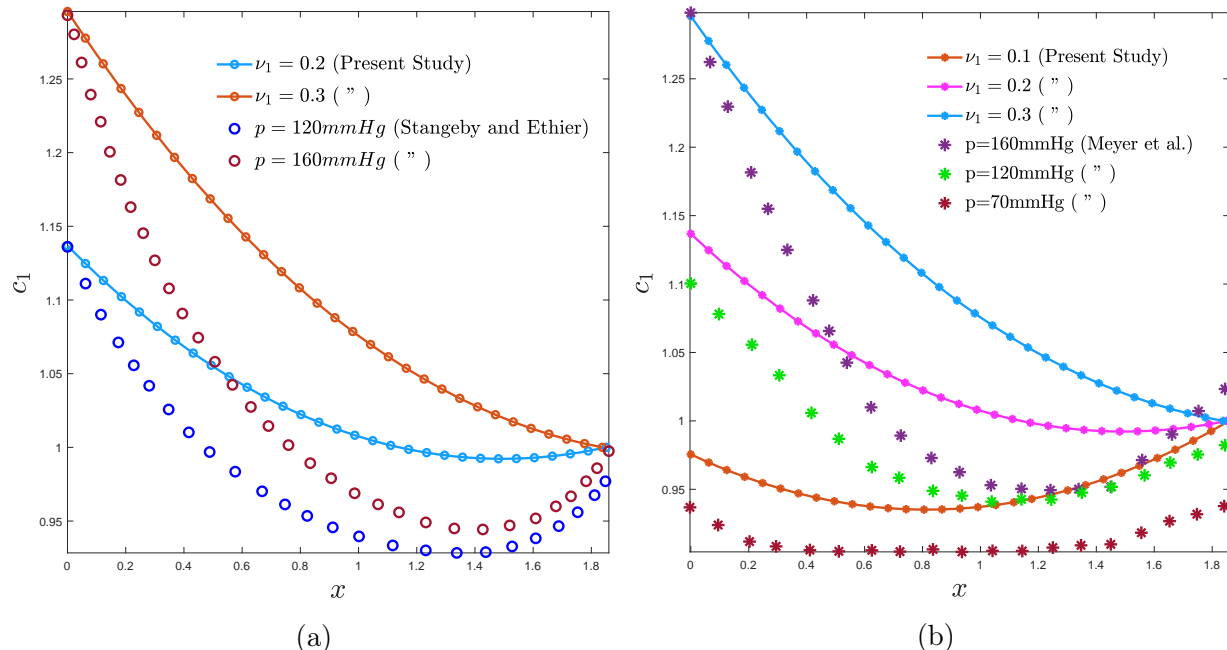


Figure 13: Comparison between the present study and the clinical studies done by (a) Stangeby and Ethier [54] and (b) Meyer et al. [46] along the variation of oxLDL concentration with distance from the intima-endothelium interface corresponding to various ν_1 for different pressures.

curs due to the overconsumption of oxLDL as it becomes toxic to macrophages. The values of most of the parameters are considered from past theoretical and clinical atherosclerosis literature in order to use in numerical simulations. The effect of oxLDL and f-cytokines, inflammatory cells (foam cell + macrophage) etc., are all systematically analyzed to illustrate the growth process represented by the change in plaque width. Our model demonstrates that the deposition of inflammatory cells starts near the endothelium and increases over time, so that plaque width within the intima grows. Our study reveals an initial step growth of the plaque width, which is followed by an exponential growth that may stabilize over time due to oxLDL-induced toxicity. The toxicity also affects the f-cytokines and inflammatory cells. As oxLDL crosses a threshold value, the inflammatory cell volume and f-cytokines concentration become constant.

We introduce three flux parameters ν_1 , ν_2 and ν_3 . The first two parameters correspond to oxLDL, while the third is for f-cytokines. The larger values for these parameters result in a larger concentration of oxLDL and f-cytokines. Consequently, the toxicity of oxLDL arises, and hence the growth of plaque width reduces for an increase in the oxLDL flux parameter. But corresponding to the increased f-cytokines flux constant, the foam cell population and plaque width increase. Furthermore, a significant change in plaque width growth is observed due to the variation in toxicity level (c_1^*). The higher toxicity simultaneously indicates mainly the death of foam cells and the proliferation of more inflammatory cells. Therefore, plaque

growth accelerates as the toxicity level increases.

The present study simplifies several complex mechanisms involved in early atherosclerosis to understand plaque formation. It is illustrated that plaque formation relies on oxLDL ingestion and macrophage chemotaxis. The role of oxLDL toxicity in plaque growth is established. The results of this study may help develop new therapeutic strategies to prevent the progression of atherosclerosis at an early stage. Besides this, the impact of High-density lipoprotein (HDL) on plaque development may be more exciting in the presence of oxLDL-induced toxicity.

Acknowledgements

First author A. S. Pramanik acknowledges University Grants Commission (UGC), Govt. of India for providing Senior Research Fellowship (NET-JRF, Award Letter Number: 1149/(CSIR-UGC NET DEC-2018)). Second author B. Dey acknowledges University Research Assistance (Ref. 1516/R-2020 dated 01.06.2020) of University of North Bengal for supporting this work.

Appendix A: Leading order coefficients

$$\varphi_n^{(0)} = 1 - \varphi_f^{(0)},$$

$$\Upsilon^{(0)} = \varphi_f^{(0)} \varphi_n^{(0)} \frac{s_0 c_1^{(0)}}{1 + s_1 c_1^{(0)}} \mathcal{H}(c_1^* - c_1^{(0)}) - \varphi_f^{(0)} \frac{s_2 + s_3 c_1^{(0)}}{1 + s_4 c_1^{(0)}} \mathcal{H}(c_1^{(0)} - c_1^*),$$

$$Q_1^{(0)} = \varphi_f^{(0)} \varphi_n^{(0)} q_0 c_1^{(0)} - \varphi_f^{(0)} \varphi_n^{(0)} q_2 c_1^{(0)},$$

$$Q_2^{(0)} = \varphi_n^{(0)} q_3 c_2^{(0)} - \varphi_n^{(0)} q_4 c_1^{(0)} c_2^{(0)},$$

$$\Sigma^{(0)} = \frac{\varphi_f^{(0)} - \varphi^*}{\left(1 - \varphi_f^{(0)}\right)^2} \mathcal{H}(\varphi_f^{(0)} - \varphi^*),$$

$$\Lambda^{(0)} = \frac{\chi}{1 + \left(\kappa c_2^{(0)}\right)^m}.$$

Appendix B: $\mathcal{O}(q_1)$ coefficients

$$\varphi_n^{(1)} = -\varphi_f^{(1)},$$

$$\begin{aligned} \Upsilon^{(1)} = & \left(\left(\varphi_f^{(0)} \varphi_n^{(1)} + \varphi_f^{(1)} \varphi_n^{(0)} \right) \frac{s_0 c_1^{(0)}}{1 + s_1 c_1^{(0)}} + \varphi_f^{(0)} \varphi_n^{(0)} \left(\frac{s_0 c_1^{(1)}}{1 + s_1 c_1^{(0)}} - \frac{s_0 s_1 c_1^{(0)} c_1^{(1)}}{\left(1 + s_1 c_1^{(0)}\right)^2} \right) \right) \mathcal{H}(c_1^* - c_1^{(1)}) \\ & - \left(\varphi_f^{(1)} \frac{s_2 + s_3 c_1^{(0)}}{1 + s_4 c_1^{(0)}} + \varphi_f^{(0)} \left(\frac{s_3 c_1^{(1)}}{1 + s_4 c_1^{(0)}} - \frac{s_4 c_1^{(1)} (s_2 + s_3 c_1^{(0)})}{\left(1 + s_4 c_1^{(0)}\right)^2} \right) \right) \mathcal{H}(c_1^{(1)} - c_1^*), \end{aligned}$$

$$\begin{aligned} Q_1^{(1)} = & \varphi_f^{(0)} \varphi_n^{(0)} q_0 \left(c_1^{(1)} - (c_1^{(0)})^2 \right) + \left(\varphi_f^{(0)} \varphi_n^{(1)} + \varphi_f^{(1)} \varphi_n^{(0)} \right) q_0 c_1^{(0)} - \varphi_f^{(0)} \varphi_n^{(0)} q_2 c_1^{(1)} \\ & - \left(\varphi_f^{(0)} \varphi_n^{(1)} + \varphi_f^{(1)} \varphi_n^{(0)} \right) q_2 c_1^{(0)}, \end{aligned}$$

$$Q_2^{(1)} = q_3 \left(\varphi_n^{(0)} c_2^{(1)} + \varphi_n^{(1)} c_2^{(0)} \right) - q_4 \varphi_n^{(0)} \left(c_1^{(0)} c_2^{(1)} + c_1^{(1)} c_2^{(0)} \right) - q_4 \varphi_n^{(1)} c_1^{(0)} c_2^{(0)},$$

$$\Sigma^{(1)} = \left(\frac{\varphi_f^{(1)}}{\left(1 - \varphi_f^{(0)}\right)^2} + \frac{2(\varphi_f^{(0)} - \varphi^*) \varphi_f^{(1)}}{\left(1 - \varphi_f^{(0)}\right)^3} \right) \mathcal{H}(\varphi_f^{(1)} - \varphi^*),$$

$$\Lambda^{(1)} = -\frac{m \chi \kappa^m \left(c_2^{(0)} \right)^{m-1} c_2^{(1)}}{\left(1 + \kappa^m \left(c_2^{(0)} \right)^m \right)^2}.$$

References

- [1] Ahmed, I.U., Byrne, H.M., Myerscough, M.R., 2022. Macrophage anti-inflammatory behaviour in a multiphase model of atherosclerotic plaque development. arXiv preprint, arXiv:2211.01867 .
- [2] Bég, O.A., Zaman, A., Ali, N., Gaffar, S.A., Bég, E.T., 2019. Numerical computation of nonlinear oscillatory two-immiscible magnetohydrodynamic flow in dual porous media system: Ftcs and fem study. Heat Transfer—Asian Research 48, 1245–1263.

- [3] Berliner, J.A., Navab, M., Fogelman, A.M., Frank, J.S., Demer, L.L., Edwards, P.A., Watson, A.D., Lusis, A.J., 1995. Atherosclerosis: basic mechanisms: oxidation, inflammation, and genetics. *Circulation* 91, 2488–2496.
- [4] Bonithon-Kopp, C., Touboul, P.J., Berr, C., Leroux, C., Mainard, F., Courbon, D., Ducimetiere, P., 1996. Relation of intima-media thickness to atherosclerotic plaques in carotid arteries: the vascular aging (eva) study. *Arteriosclerosis, Thrombosis, and Vascular biology* 16, 310–316.
- [5] Breward, C., Byrne, H., Lewis, C., 2002. The role of cell-cell interactions in a two-phase model for avascular tumour growth. *Journal of Mathematical Biology* 45, 125–152.
- [6] Breward, C.J., Byrne, H.M., Lewis, C.E., 2003. A multiphase model describing vascular tumour growth. *Bulletin of Mathematical Biology* 65, 609–640.
- [7] Byrne, H.M., King, J.R., McElwain, D.S., Preziosi, L., 2003. A two-phase model of solid tumour growth. *Applied Mathematics Letters* 16, 567–573.
- [8] Calvez, V., Ebde, A., Meunier, N., Raoult, A., 2009. Mathematical modelling of the atherosclerotic plaque formation, in: *Esaim: Proceedings, EDP Sciences*. pp. 1–12.
- [9] Calvez, V., Houot, J.G., Meunier, N., Raoult, A., Rusnakova, G., 2010. Mathematical and numerical modeling of early atherosclerotic lesions, in: *ESAIM: Proceedings, EDP Sciences*. pp. 1–14.
- [10] Chalmers, A.D., Bursill, C.A., Myerscough, M.R., 2017. Nonlinear dynamics of early atherosclerotic plaque formation may determine the efficacy of high density lipoproteins (hdl) in plaque regression. *PLoS One* 12, e0187674.
- [11] Chalmers, A.D., Cohen, A., Bursill, C.A., Myerscough, M.R., 2015. Bifurcation and dynamics in a mathematical model of early atherosclerosis. *Journal of Mathematical Biology* 71, 1451–1480.
- [12] Channon, K.M., 2006. The endothelium and the pathogenesis of atherosclerosis. *Medicine* 34, 173–177.
- [13] Chatzizisis, Y.S., Coskun, A.U., Jonas, M., Edelman, E.R., Feldman, C.L., Stone, P.H., 2007. Role of endothelial shear stress in the natural history of coronary atherosclerosis and vascular remodeling: molecular, cellular, and vascular behavior. *Journal of the American College of Cardiology* 49, 2379–2393.
- [14] Chen, D., Roda, J.M., Marsh, C.B., Eubank, T.D., Friedman, A., 2012. Hypoxia inducible factors-mediated inhibition of cancer by gm-csf: a mathematical model. *Bulletin of Mathematical Biology* 74, 2752–2777.
- [15] Cilla, M., Pena, E., Martinez, M.A., 2014. Mathematical modelling of atheroma plaque formation and development in coronary arteries. *Journal of The Royal Society Interface* 11, 20130866.

- [16] Cobbold, C., Sherratt, J., Maxwell, S., 2002. Lipoprotein oxidation and its significance for atherosclerosis: a mathematical approach. *Bulletin of Mathematical Biology* 64, 65–95.
- [17] Cohen, A., Myerscough, M.R., Thompson, R.S., 2014. Athero-protective effects of high density lipoproteins (hdl): an ode model of the early stages of atherosclerosis. *Bulletin of Mathematical Biology* 76, 1117–1142.
- [18] Cunningham, K.S., Gotlieb, A.I., 2005. The role of shear stress in the pathogenesis of atherosclerosis. *Laboratory Investigation* 85, 9–23.
- [19] Davies, M., Woolf, N., 1993. Atherosclerosis: what is it and why does it occur? *British Heart Journal* 69, S3.
- [20] Dey, B., Raja Sekhar, G.P., 2016. Hydrodynamics and convection enhanced macromolecular fluid transport in soft biological tissues: Application to solid tumor. *Journal of Theoretical Biology* 395, 62–86.
- [21] El Khatib, N., Génieys, S., Kazmierczak, B., Volpert, V., 2009. Mathematical modelling of atherosclerosis as an inflammatory disease. *Philosophical Transactions of the Royal Society A: Mathematical, Physical and Engineering Sciences* 367, 4877–4886.
- [22] El Khatib, N., Génieys, S., Kazmierczak, B., Volpert, V., 2012. Reaction–diffusion model of atherosclerosis development. *Journal of Mathematical Biology* 65, 349–374.
- [23] El Khatib, N., Génieys, S., Volpert, V., 2007. Atherosclerosis initiation modeled as an inflammatory process. *Mathematical Modelling of Natural Phenomena* 2, 126–141.
- [24] Filipovic, N., Teng, Z., Radovic, M., Saveljic, I., Fotiadis, D., Parodi, O., 2013. Computer simulation of three-dimensional plaque formation and progression in the carotid artery. *Medical & Biological Engineering & computing* 51, 607–616.
- [25] Furchgott, R.F., 1999. Endothelium-derived relaxing factor: discovery, early studies, and identification as nitric oxide. *Bioscience Reports* 19, 235–251.
- [26] Grootaert, M.O., da Costa Martins, P.A., Bitsch, N., Pintelon, I., De Meyer, G.R., Martinet, W., Schrijvers, D.M., 2015. Defective autophagy in vascular smooth muscle cells accelerates senescence and promotes neointima formation and atherogenesis. *Autophagy* 11, 2014–2032.
- [27] Gui, T., Shimokado, A., Sun, Y., Akasaka, T., Muragaki, Y., 2012. Diverse roles of macrophages in atherosclerosis: from inflammatory biology to biomarker discovery. *Mediators of Inflammation* 2012.
- [28] Han, K., Hong, K., Park, J., Ko, J., Kang, D., Park, S., 2004. Crp promotes mcp-1 mediated chemotaxis through upregulating ccr2 expression in human monocytes. *Circulation* 109, 2566–2571.

- [29] Hansson, G.K., Libby, P., 2006. The immune response in atherosclerosis: a double-edged sword. *Nature Reviews Immunology* 6, 508–519.
- [30] Hansson, G.K., Robertson, A.K.L., Söderberg-Nauclér, C., 2006. Inflammation and atherosclerosis. *Annual Review of Pathology: Mechanisms of Disease* 1, 297–329.
- [31] Hao, W., Friedman, A., 2014. The ldl-hdl profile determines the risk of atherosclerosis: a mathematical model. *PloS One* 9, e90497.
- [32] Hegyi, L., Skepper, J.N., CARY, N.R., MITCHINSON, M.J., 1996. Foam cell apoptosis and the development of the lipid core of human atherosclerosis. *The Journal of Pathology* 180, 423–429.
- [33] Hillen, T., Painter, K.J., 2009. A user’s guide to pde models for chemotaxis. *Journal of Mathematical Biology* 58, 183–217.
- [34] Hoffmann, K.A., Chiang, S.T., 2000. *Computational fluid dynamics volume i. Engineering Education System* .
- [35] Ibragimov, A., McNeal, C., Ritter, L., Walton, J., 2005. A mathematical model of atherogenesis as an inflammatory response. *Mathematical Medicine and Biology* 22, 305–333.
- [36] Kim, Y., Friedman, A., 2010. Interaction of tumor with its micro-environment: A mathematical model. *Bulletin of Mathematical Biology* 72, 1029–1068.
- [37] Korshunov, V.A., Schwartz, S.M., Berk, B.C., 2007. Vascular remodeling: hemodynamic and biochemical mechanisms underlying glagov’s phenomenon. *Arteriosclerosis, Thrombosis, and Vascular Biology* 27, 1722–1728.
- [38] Kumar, P., Dey, B., Raja Sekhar, G.P., 2018. Nutrient transport through deformable cylindrical scaffold inside a bioreactor: an application to tissue engineering. *International Journal of Engineering Science* 127, 201–216.
- [39] Lee, T., Baines, M.J., Langdon, S., Tindall, M.J., 2013. A moving mesh approach for modelling avascular tumour growth. *Applied Numerical Mathematics* 72, 99–114.
- [40] Lemon, G., King, J.R., Byrne, H.M., Jensen, O.E., Shakesheff, K.M., 2006. Mathematical modelling of engineered tissue growth using a multiphase porous flow mixture theory. *Journal of Mathematical Biology* 52, 571–594.
- [41] Libby, P., Ridker, P.M., Maseri, A., 2002. Inflammation and atherosclerosis. *Circulation* 105, 1135–1143.
- [42] Liu, L.K., Lee, H.J., Shih, Y.W., Chyau, C.C., Wang, C.J., 2008. Mulberry anthocyanin extracts inhibit ldl oxidation and macrophage-derived foam cell formation induced by oxidative ldl. *Journal of Food Science* 73, H113–H121.

- [43] Lusis, A., 2000. Atherosclerosis. *Nature* 407, 233–241.
- [44] Marchant, C.E., Van Der Wen, C., Law, N.S., Hardwick, S.J., Carpenter, K.L., Mitchinson, M.J., 1996. Oxidation of low-density lipoprotein by human monocyte-macrophages results in toxicity to the oxidising culture. *Free Radical Research* 24, 333–342.
- [45] McKay, C., McKee, S., Mottram, N., Mulholland, T., Wilson, S., Kennedy, S., Wadsworth, R., 2005. Towards a model of atherosclerosis. University of Strathclyde , 1–29.
- [46] Meyer, G., Merval, R.g., Tedgui, A., 1996. Effects of pressure-induced stretch and convection on low-density lipoprotein and albumin uptake in the rabbit aortic wall. *Circulation Research* 79, 532–540.
- [47] Mow, V.C., Holmes, M.H., Lai, W.M., 1984. Fluid transport and mechanical properties of articular cartilage: a review. *Journal of Biomechanics* 17, 377–394.
- [48] Navab, M., Ananthramaiah, G., Reddy, S.T., Van Lenten, B.J., Ansell, B.J., Fonarow, G.C., Vahabzadeh, K., Hama, S., Hough, G., Kamranpour, N., et al., 2004. Thematic review series: the pathogenesis of atherosclerosis the oxidation hypothesis of atherogenesis: the role of oxidized phospholipids and hdl. *Journal of Lipid Research* 45, 993–1007.
- [49] Newby, A.C., Zaltsman, A.B., 1999. Fibrous cap formation or destruction—the critical importance of vascular smooth muscle cell proliferation, migration and matrix formation. *Cardiovascular Research* 41, 345–360.
- [50] Ougrinovskaia, A., Thompson, R.S., Myerscough, M.R., 2010. An ode model of early stages of atherosclerosis: mechanisms of the inflammatory response. *Bulletin of Mathematical Biology* 72, 1534–1561.
- [51] Prakash, J., Raja Sekhar, G.P., De, S., Böhm, M., 2010. A criterion to avoid starvation zones for convection–diffusion–reaction problem inside a porous biological pellet under oscillatory flow. *International Journal of Engineering Science* 48, 693–707.
- [52] Ross, R., 1999. Atherosclerosis—an inflammatory disease. *New England Journal of Medicine* 340, 115–126.
- [53] Roth, G.A., Abate, D., Abate, K.H., Abay, S.M., Abbafati, C., Abbasi, N., Abbastabar, H., Abd-Allah, F., Abdela, J., Abdelalim, A., et al., 2018. Global, regional, and national age-sex-specific mortality for 282 causes of death in 195 countries and territories, 1980–2017: a systematic analysis for the global burden of disease study 2017. *The Lancet* 392, 1736–1788.
- [54] Stangeby, D.K., Ethier, C.R., 2002. Coupled computational analysis of arterial ldl transport—effects of hypertension. *Computer Methods in Biomechanics & Biomedical Engineering* 5, 233–241.

- [55] Watson, M.G., Byrne, H.M., Macaskill, C., Myerscough, M.R., 2018. A two-phase model of early fibrous cap formation in atherosclerosis. *Journal of Theoretical Biology* 456, 123–136.
- [56] Watson, M.G., Byrne, H.M., Macaskill, C., Myerscough, M.R., 2020. A multiphase model of growth factor-regulated atherosclerotic cap formation. *Journal of Mathematical Biology* 81, 725–767.
- [57] Wu, M.Y., Li, C.J., Hou, M.F., Chu, P.Y., 2017. New insights into the role of inflammation in the pathogenesis of atherosclerosis. *International Journal of Molecular Sciences* 18, 2034.
- [58] Zaman, A., Ali, N., Bég, O.A., 2016. Unsteady magnetohydrodynamic blood flow in a porous-saturated overlapping stenotic artery—numerical modeling. *Journal of Mechanics in Medicine and Biology* 16, 1650049.